

Spatial log-Gaussian Cox process models and sampling paths: Toward optimal design

Kenneth Flagg^{a,*}, John Borkowski^a, Andrew Hoegh^a

^a*Department of Mathematical Sciences, Montana State University, Bozeman, MT 59717*

Abstract

The log-Gaussian Cox (LGCP) process model is becoming the go-to model for spatial point pattern data as fast Bayesian computing methods are removing the barriers to their use. In many applications, such as unexploded ordnance remediation and species distribution studies, a sampling procedure is used in which only events near a one-dimensional path are observed. Very little work has been done regarding optimal design of these paths. We present a variety of path designs and user simulations to compare them in terms of model-based spatial prediction criteria. We also define a spatial coverage statistic for path designs, the average distance-to-path. We show that, when total length is limited, paths with regular spacing and direction changes provide small errors and low posterior variance while being relatively robust against computational artifacts. For longer paths, systematic line-transect designs perform well.

Keywords: spatial point process, log-Gaussian Cox process, optimal sampling, model-based design, spatial sampling design

1. Introduction

Spatial point process models have generally been infeasible because of their computational demands, but recent advances in Bayesian computing have made the Log-Gaussian Cox process (LGCP) an attainable model in practice (Rue et al., 2009; Lindgren et al., 2011; Illian et al., 2012; Simpson et al., 2016). These

*Corresponding author
Email address: kenneth.flagg@montana.edu (Kenneth Flagg)

advances make it possible to fit LGCP models easily, without time-consuming Monte Carlo methods. In some applications, the entire point pattern is not fully observed due to variable sampling effort. This is referred to as a degraded point pattern (Chakraborty et al., 2011). It is relatively simple to accommodate
10 variable sampling effort in these models using modern Bayesian computing tools (Yuan et al., 2017). However, the literature on optimal sampling for spatial point process models is in its infancy (Liu and Vanhatalo, 2020).

Point pattern data are routinely collected in species distribution studies and ordnance response projects. The data consist of the locations of events in some
15 spatial region. In many cases it is too costly to observe the entire study, region so a sampling procedure is employed. These applications may use quadrat sampling or line-transect sampling, with transect sampling being more common. Software is now available to fit spatial point process models to data acquired via distance sampling and simultaneously estimate the detection function (Johnson et al.,
20 2014; R Core Team, 2020). Various spatial mapping procedures have been used to map where events occur in space. However, these have traditionally involved aggregating the data to grid cell counts or computing moving averages. Aggregation has the downside of introducing arbitrary structure into the data by the choice of grid scheme or averaging window, and requires unnecessary computation effort (Simpson et al., 2016).
25

In ecological settings, sampling plans are often designed around the goal of estimating total abundance. Ordnance response surveys are typically designed to provide enough data to detect (but not necessarily map) intensity hotspots (USACE, 2015; Flagg et al., 2020). However, to our knowledge, there
30 has been very little work done in deciding *where* to collect data when the goal is to map the intensity using a spatial point process model. While some ideas about the characteristics of a good point design apply to paths, creating an optimal path design is not as simple as connecting the points of a point design with line segments. There are many ways to connect points into a path, so optimal
35 design criteria must apply to the whole path and not only to the waypoints.

In this paper, we develop a space-filling criterion for path designs, present a

variety of sampling path designs, and assess their utility for spatial prediction using LGCP model fitting in terms of robustness to computational issues and model-based optimality for prediction.

40 1.1. *Log-Gaussian Cox process*

The log-Gaussian Cox process (LGCP) is an inhomogeneous Poisson process where the logarithm of the intensity function is a Gaussian process (Møller et al., 1998). The LGCP model provides a flexible model for mapping event intensity over space using few parameters. Efficient Bayesian computation tools 45 are available using INLA to approximate the posterior marginal distributions (Rue et al., 2009), a finite element approach to represent the Gaussian process (Lindgren et al., 2011), and pseudodata to approximate the point process likelihood (Simpson et al., 2016).

1.2. *Spatial design*

50 Most classical sampling and design work has been done for points, or for small quadrats approximated as points, rather than for paths. In two-dimensional geostatistical model-based design, regular spacing is optimal for spatial prediction but randomness and a variety of interpoint distances are best for parameter estimation (Diggle and Lophaven, 2006). Inhibitory plus close pairs designs are a 55 good compromise when estimation and prediction are both important (Chipeta et al., 2017).

Design-based approaches exist to spread points through high-dimensional design spaces (Borkowski and Piepel, 2009), and Latin hypercube sampling has space-filling characteristics (McKay et al., 1979; Hussian et al., 2011). Minimax 60 and maximin distance are popular criteria for ensuring design points represent the entirety of a large (or high-dimensional) design space (Johnson et al., 1990). These criteria are calculated from the distances between design points and arbitrary points in the design space, explicitly ensuring coverage by minimizing the maximum distance between the design space and the design (minimax) or 65 maximizing the minimum distance between pairs of design points (maximin).

1.3. Space-filling curves

A relevant area of mathematical research is in deterministic space-filling curves. These have been used in the design of dense or stretchable circuits (Ogorzałek, 2009; Ma and Zhang, 2016) and high-dimensional data visualization in bioinformatics (Anders, 2009). They are appealing as path designs because, given enough length, the path will visit every part of the study site.

Example space-filling curves include the Hilbert curve, which is simple to construct, and the Peano curve, which is very flexible for filling irregular shapes (Fan et al., 2014). Space-filling curves are one-dimensional paths constructed iteratively; as the number of iterations goes to infinity, the limiting path has nonzero area and actually fills the space (Sagan, 1994). For applications we stop after a finite number of iterations.

1.4. Paths as sampling designs

The small body of literature on spatial sampling design for point pattern data has focused on line transects. Pollard et al. (2002) began with line transects and adaptively added zigzags in a species abundance survey.

The Visual Sample Plan software includes features to create systematic transect plans and augment plans with additional transects in regions lacking spatial coverage (Matzke et al., 2014). It helps the user choose the transect spacing to maximize the probability of detecting the presence of a hotspot of specified size and intensity. However, it does not employ criteria to optimize spatial prediction.

Liu and Vanhatalo (2020) provided one of the first explicit discussions of design in the context of spatial LGCP models. The study used narrow quadrats (swaths along line-transects) as the sampling units. The transects were short relative to the size of the study region and not connected into a path, so they were treated as disconnected points for the purposes of design construction.

1.5. Goals of this paper

We have two broad goals for this paper. First, we will illuminate the current state of practical computing for LGCP models fit to degraded point patterns

observed via survey sampling. Second, we open discussion of path design for LGCP models by identifying design schemes with promise for field use.

We accomplish these goals via a simulation study, using many designs each applied to the same simulated datasets. The simulated data collection procedure is based upon geomagnetic surveys for unexploded ordnance, where metal detectors traverse a path and detect events under their footprint, i.e. within a (fixed and assumed known) width centered on the path. The paths are long enough that they cannot be approximated by discrete design points.

2. Materials and methods

With an eye toward practical considerations of data collection, we present criteria to compare sampling strategies that impact LGCP model fitting and posterior inferences. We compare plans with (approximately) fixed path lengths, most of which avoid sharp turns. Data collection equipment (e.g. vehicle-towed metal detectors) may have limited mobility, requiring minimizing the number or angle of turns. This section describes the designs in detail, then introduces notation and design criteria, and finally summarizes the computational model-fitting approach.

2.1. Sampling design schemes

In this section, we present three variations of parallel line transect designs and three schemes that produce more complex designs. To clarify terminology, a *path* or *design* is a realized set of one or more connected components with length but not area. The paths considered in this work are constructed as sequences of line segments. A *design scheme*, or simply *scheme*, is a procedure for generating designs with some shared characteristics. Figure 1 illustrates a selection of designs from these schemes.

2.1.1. Parallel line transects

Parallel straight-line transects are common in ordnance response studies and in ecological studies using distance sampling. Systematic designs are common

because they provide good spatial coverage in the sense that any point in the
125 study site has an a priori known maximum distance from the path. For point designs, systematic designs are optimal for prediction, simple random samples are optimal for estimation, and inhibitory with close pairs designs are becoming a popular compromise (Chipeta et al., 2017). We adapt all three of these to the parallel line transect setting. We use line transects running north-south,
130 with three methods of choosing the horizontal coordinate: simple random sample (SRS), systematic with a random starting point and fixed spacing, and inhibitory plus close pairs. Figure 1 (left column) shows an example of each scheme with 25 transects. Additional examples appear in Appendix Appendix C.

135 *2.1.2. Parallel serpentine transects*

One simple way to observe a greater variety of locations and different directions is to add lateral “zigzags” to transects. We include alternate right and left turns at right angles to create serpentine transects. This could decrease prediction variance because more of the path will be close to each point in the study
140 area than would be under a line transect design with similar total distance. They will also improve estimation of the covariance function in the presence of anisotropy. Figure 1, top right, shows two examples.

2.1.3. Latin hypercube sampling

Random Latin hypercube sampling (LHS) produces a design that spreads
145 discrete points through a (potentially high-dimensional) design space, ensuring that the full range of each dimension is included while remaining balanced and keeping the number of points small (McKay et al., 1979). This is done by partitioning each dimension into a specified number k of intervals (thus stratifying a d -dimensional design space into k^d cells), selecting a Latin hypercube
150 design to determine which k cells will contain a design point, and then drawing each design point from a uniform distribution over its cell. In two dimensions, this scheme produces point designs with good spatial coverage properties. We

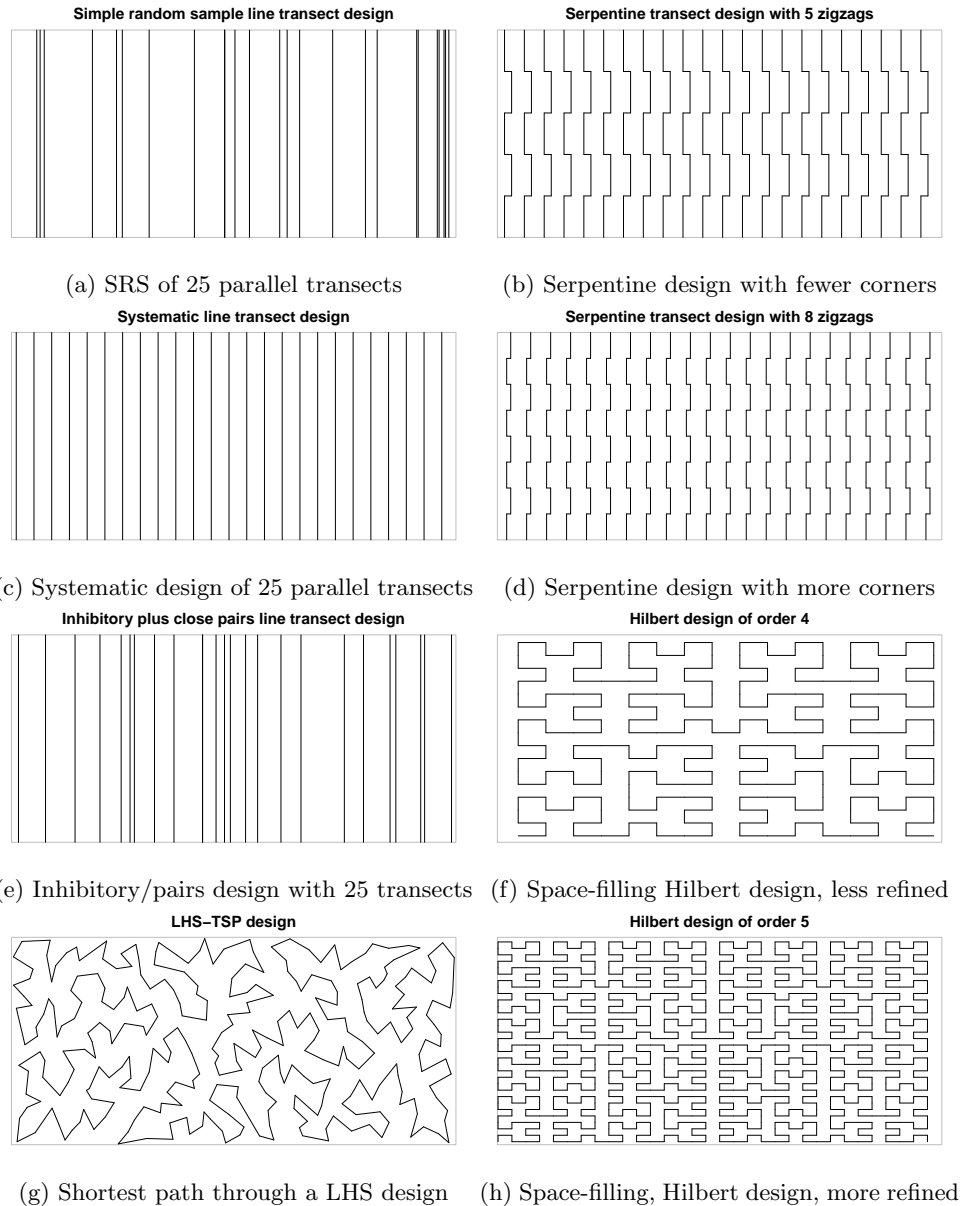


Figure 1: Examples of plans from six design schemes. Except for the Hilbert curve of order 5, all of these plans have approximately the same total length.

use the LHS design as waypoints for a path. Because longer distance typically brings increased costs, we treat this as a traveling salesperson problem (TSP) and use the shortest path through the waypoints as our design. This
155 LHS-TSP scheme produces paths that have many sharp corners but leaves few large voids (example in Figure 1, bottom left). Waypoints are generated by the `lhs` R package (Carnell, 2020) and connected into a shortest path by the TSP package (Hahsler and Hornik, 2020). A downside of this design scheme is that
160 the length cannot be specified directly, and only certain distances are possible depending on the number of bins used.

2.1.4. Space-filling curves

As a representative of space-filling curves, we use the Hilbert curve scaled to fit the study site. These designs have many short segments meeting at right
165 angles. The only parameter of this design scheme is the order, or number of iterations used in refining the curve. Each iteration increases the length and complexity of the design. This produces a deterministic design, so a random offset is added to vary which points are observed. The Hilbert curve is generated by the `HilbertVis` R package (Anders, 2009).

170 2.1.5. Spatial coverage criterion

One critically important characteristic of a spatial design is the concept of spatial coverage, or how well the design represents the study site in the sense that all points in the region are close to observed locations. The criterion we propose to measure this is the average distance to the path. We define the
175 distance between a point and the path as the distance between that point and the nearest point on the path, then take the average over all points in the study region. This can be roughly understood as the radius of a typical unsurveyed void.

2.2. LGCP model and notation

180 The full point process is denoted \mathbf{X} and operates over the entire study site \mathcal{R} . The full realized point pattern is denoted \mathbf{x} and is a finite (countable) subset

of \mathbf{R} . However, only a subregion of \mathcal{R} is surveyed. This subregion is \mathcal{S} , the set of all points within a specified radius of the survey path. The observed point pattern is defined as $\mathbf{x}_{\mathcal{S}} = \mathbf{x} \cap \mathcal{S}$.

In the LGCP model, \mathbf{X} is a Poisson process with intensity function $\lambda(u)$, $u \in \mathcal{R}$. This intensity function is itself a stochastic process, modeled on the natural logarithm scale as

$$\log[\lambda(u)] = \mu + \mathbf{e}(u), \quad (1)$$

¹⁸⁵ with an intercept μ and spatial error term $\mathbf{e}(u)$. The error term is a Gaussian process with mean 0 and covariance function $C(u, v)$. In our simulation study, C is a stationary and isotropic Matérn covariance function with smoothness parameter ν , spatial scale ρ , and variance σ^2 .

2.2.1. Model-based criteria

¹⁹⁰ For model-based comparisons, we compare the posterior distribution of the intercept μ to the realized mean of the simulated GP, and evaluate two spatial prediction criteria. For the intercept, we simply record whether the 95% central interval captures the realized mean. This is aggregated into the capture rate for scheme.

The spatial prediction criteria that we evaluate are the mean squared prediction error (MSPE) of the log intensity surface,

$$E[(\mu + \mathbf{e}(u) - \log[\lambda(u)])^2 | \mathbf{x}_{\mathcal{S}}], \quad (2)$$

and the average prediction variance (APV) of the latent Gaussian process,

$$\text{Var}[\mathbf{e}(u) | \mathbf{x}_{\mathcal{S}}]. \quad (3)$$

¹⁹⁵ In the above notation, λ is the true realized intensity function, which is known in the simulations.

The capture rate of the mean describes accuracy in the overall scale of the intensity surface. Inaccuracy in the mean implies that that model will predict overall too many or too few events. The other criteria reflect two important

200 characteristics of a useful spatial prediction. First, deviation from the true surface should be low, and is indicated by low MSPE. Second, the model's own assessment of prediction uncertainty will be used in practice to build trust in the inferences, so low APV is desirable.

2.2.2. Model fitting

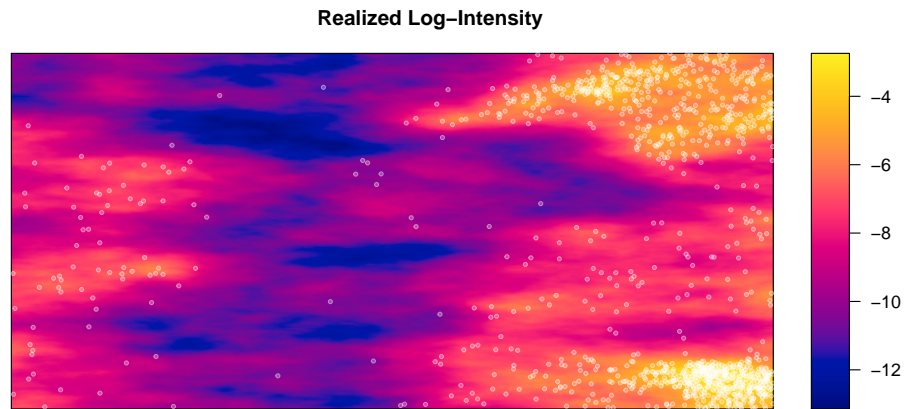
205 We fit the spatial LGCP model using nested integrated Laplace approximations and the R-INLA package (Rue et al., 2009; Blangiardo and Cameletti, 2015). We used the `inla()` function with its default optimizer parameters. The Gaussian process is approximated using a finite element approach (Lindgren et al., 2011). The point pattern is modeled by pseudodata placed at the events 210 and the finite element nodes (Simpson et al., 2016). When using an adequate finite element mesh, this procedure allows fast and accurate approximation of the posterior distribution.

3. Simulation study

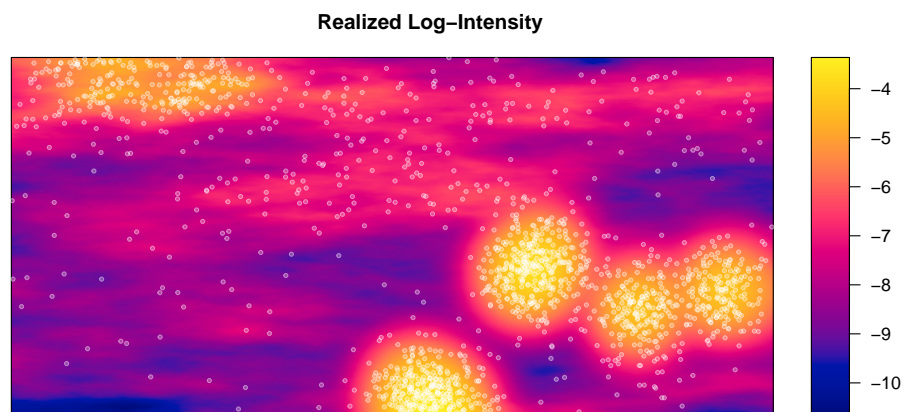
We compare the design schemes by applying multiple designs from each 215 scheme to the same simulated datasets. There are two data-generating models and five datasets generated from each, for a total of ten datasets (Section 3.1). We will focus on two illustrative datasets when presenting the results. We use 8 schemes at four levels of survey effort, and 100 designs generated from each scheme at each effort level (Section 3.2). All events within a 2 unit radius of 220 the path are observed. The same model is fit to each observed point pattern (Section 3.3).

3.1. Study site

We consider a fictitious site \mathcal{R} with the simple shape of a 1500 unit by 700 unit rectangle. In this site, we simulate two data generating models that produce 225 random intensity functions with hotspots. First, a LGCP with latent GP mean $\mu = \log(250/|\mathcal{R}|) = -8.34$ and Matérn covariance function with $\nu = 1$, $\sigma = 2$, and range = 200. This model produces relatively unstructured hotspots due to



(a) Realized LGCP log-intensity



(b) Realized LGCP with Clusters log-intensity

Figure 2: The realized intensity function (natural log scale) and complete point pattern from a LGCP, and from a LGCP superposed with a cluster process.

large variability in the GP. Figure 2a shows an example realization from this process.

Second, a two-stage cluster process and a LGCP are superposed. The cluster process (a Neyman-Scott or, more specifically, Thomas process) is constructed as follows. The number of clusters is Poisson-distributed with mean 3. The number of events per cluster is Poisson-distributed with mean 200. The cluster centers are distributed uniformly over \mathcal{R} . Events come from a bivariate normal distribution with mean equal to the cluster center and variance $\Sigma = \tau^2 \mathbf{I}$, $\tau = 50$. The LGCP component has $\mu = \log(250/|\mathcal{R}|) = -8.34$ and Matérn covariance with $\nu = 1$, $\sigma = 1$, and range = 200. This model is based upon the typical conceptual model of a firing range, with a background process (represented by the LGCP) and a small number of higher-intensity foreground clusters containing the events of interest (example in Figure 2b). As a shorthand, we refer to this generative process as LGCP with Clusters.

The LGCP generating process matches the model fit to the realized data. The model should both produce accurate predictions and have low bias in the posterior means of the parameters. On the other hand, the parameters of the LGCP with Clusters process will not correspond to the LGCP model parameters, but we anticipate that in general the latent GP in the LGCP model will still accurately predict the log-intensity function.

3.2. Path design schemes

The simulation uses each of the design schemes discussed in Section 2.1. The surveyed region \mathcal{S} consists of all points within 2 units of the design. That is, \mathcal{S} is a collection of strips along each segment of the design. All events within 2 units of the design are observed and all events farther than 2 units from the path are unobservable.

The design parameters for each scheme are varied to create four different levels of survey effort: low, medium, high, and very high. Within each effort level, the total length or distance traveled is comparable across all schemes. The inhibitory plus close pairs scheme and the serpentine scheme are further

Table 1: Design schemes used in the simulation study. The table presents the design parameters, distance travelled along the path, percent of the study area surveyed, and average distance to the path under each of four survey effort levels. The average distance to the path varies due from design to design, and is presented as average (SD).

* Variable area due to overlapping segments, reported as average (SD).

** Variable distance surveyed, reported as average (SD).

Scheme	Low Effort	Medium Effort	High Effort	Very High Effort
SRS	10 transects Length: % Surveyed: Avg. Dist. to Path:	25 transects 7000 units 6.46% (0.202%)* 29.7 (6.01)	50 transects 35000 units 12.5% (0.331%)* 15.0 (1.99)	70 transects 49000 units 17.2% (0.459%)* 10.8 (1.44)
Systematic	10 transects Length: % Surveyed: Avg. Dist. to Path:	25 transects 7000 units 2.68% 6.70% 38.4 (0.866)	50 transects 35000 units 13.4% 7.56 (0.0307)	70 transects 49000 units 18.7% 5.40 (0.0164)
Inhibitory, 10% Close Pairs	9 transects 1 paired Length: % Surveyed: Avg. Dist. to Path:	23 transects 2 paired 7000 units 6.53% (0.172%)* 20.8 (1.82)	45 transects 5 paired 35000 units 12.8% (0.314%)* 10.6 (1.24)	63 transects 7 paired 49000 units 17.5% (0.427%)* 7.64 (0.576)
Inhibitory, 20% Close Pairs	8 transects 2 paired Length: % Surveyed: Avg. Dist. to Path:	20 transects 5 paired 7000 units 6.56% (0.157%)* 22.0 (2.97)	40 transects 10 paired 35000 units 12.8% (0.303%)* 11.4 (1.70)	56 transects 14 paired 49000 units 17.6% (0.368%)* 8.26 (0.826)
Serpentine, 5 Zigzags	7 transects 75 unit offset Length: % Surveyed: Avg. Dist. to Path:	22 transects 23.9 unit offset 7000 units 6.68% 43.2 (1.83)	47 transects 11.2 unit offset 35000 units 13.4% 7.79 (0.0508)	67 transects 7.84 unit offset 49000 units 18.7% 5.51 (0.0309)
Serpentine, 8 Zigzags	7 transects 42.9 unit offset Length: % Surveyed: Avg. Dist. to Path:	22 transects 13.6 unit offset 7000 units 6.67% 44.5 (2.03)	47 transects 6.38 unit offset 35000 units 13.3% 7.76 (0.0328)	67 transects 4.48 unit offset 49000 units 18.7% 5.50 (0.0271)
LHS-TSP	50 bins Length: % Surveyed: Avg. Dist. to Path:	300 bins 7177 (189) units** 2.73% (0.0722%)** 43.5 (1.44)	1200 bins 17191 (168) units** 6.51% (0.0632%)** 17.4 (0.186)	2400 bins 34196 (225) units** 12.9% (0.0835%)** 8.63 (0.0683) 48433 (342) units** 18.2% (0.127%)** 6.08 (0.0562)
Hilbert Curve	3rd Order Length: % Surveyed: Avg. Dist. to Path:	4th Order 8581 units 3.27% 37.3 (1.95)	5th Order 17442 units 6.634% 17.9 (0.480)	6th Order 35025 units 13.3% 8.77 (0.113) 70121 units 26.47% 4.37 (0.0382)

varied to employ different numbers of pairs and different numbers of zigzags, respectively. Table 1 provides an overview of the different settings.

260 The parallel line transect schemes have transects running north-south, with the effort level determining the number of transects. We expect the simple random sample scheme to produce high prediction variance and large prediction error in big gaps between transects. The systematic sample scheme uses a uniformly-distributed starting point and constant spacing between adjacent 265 transects. We expect systematic transects to provide accurate inferences for the intensity surface and moderate prediction variance.

270 For the inhibitory plus close pairs line transect scheme, we vary the numbers of paired and unpaired transects. The total number of transects is the same as in the SRS and systematic designs, but 10% and 20% of the transects (rounded 275 to the nearest integer) are designated as redundant members of a pair. The remaining primary transects are placed according to a one-dimensional Strauss process (Strauss, 1975; Kelly and Ripley, 1976). The Strauss attraction parameter is set at $\gamma = 0.05$ and the radius for counting pairs is 1500 units divided by the total number of transects. Then each redundant transect is randomly paired to a primary transect, and placed within the pair radius of the primary 280 transect according to a uniform distribution. We expect this scheme to have intermediate performance between the simple random sample and the systematic line transect schemes.

285 The serpentine transect scheme has transects running north-south with constant east-west spacing and a random starting point for the first transect. The number of zigzags (north-south segments) is 5 or 8 per transect. The designs are constructed to have the same length as the line-transect designs: there are three fewer serpentine transects, and the perpendicular offset is set so the total east-west distance equals the length of three north-south line transects. These 290 designs should result in smaller prediction errors and lower variance farther from the path, compared to line-transect designs.

Our Latin hypercube sampling/traveling salesperson (LHS-TSP) scheme uses a different number of bins for each effort level (see Table 1). Preliminary

experimentation found that these bin numbers produced total lengths similar to
290 the transect schemes. The LHS-TSP scheme is expected to result in small pre-
diction errors and low prediction variance per unit distance traveled. However,
the designs will have many sharp corners and may leave some large voids.

The Hilbert curve scheme uses a random starting point and a Hilbert curve
295 of order 3, 4, 5, or 6. The path length is a deterministic function of the order
and differs greatly among curves of different orders. These orders yield lengths
similar to the lengths of the transect designs. Hilbert designs should provide
low prediction variance, but have lots of short segments.

3.3. Model specification

The same Bayesian LGCP model is fit to each observed dataset. The ob-
300 served point pattern \mathbf{x} is a realization of \mathbf{X} , a Poisson process on \mathcal{R} with intensity
 $\lambda(u)$. The intensity is modeled as $\log[\lambda(u)] = \mu + \mathbf{e}(u)$. The spatial error term \mathbf{e}
is a Gaussian process with mean $\mathbf{0}$ and a Matérn covariance function with fixed
 $\nu = 1$.

The intercept μ has a $\text{Unif}(-\infty, \infty)$ prior. The covariance parameters σ and
305 ρ have a PC prior with $\Pr(\sigma > 3) = 0.1$ and $\Pr(\rho < 100) = 0.1$ (Fuglstad et al.,
2019; Simpson et al., 2017).

3.4. Finite element mesh

The Gaussian process prediction surface is approximated on the finite ele-
310 ment mesh shown in Figure 3. The GP is predicted at the 298 nodes (black
dots on the plot) and is linearly interpolated elsewhere. The nodes are weighted
according to the area of their dual cells (grey outlines) and used for numerical
integration of the likelihood (Lindgren et al., 2011).

The choice of mesh is important because a mesh that is too coarse can-
not represent small-scale structures and thus will incur large approximation
315 errors. On the other hand, the mesh has implications for computation because
the nodes and the observed events correspond to pseudodata points. In our
sparsely-observed point pattern setting, the number of mesh nodes will be large

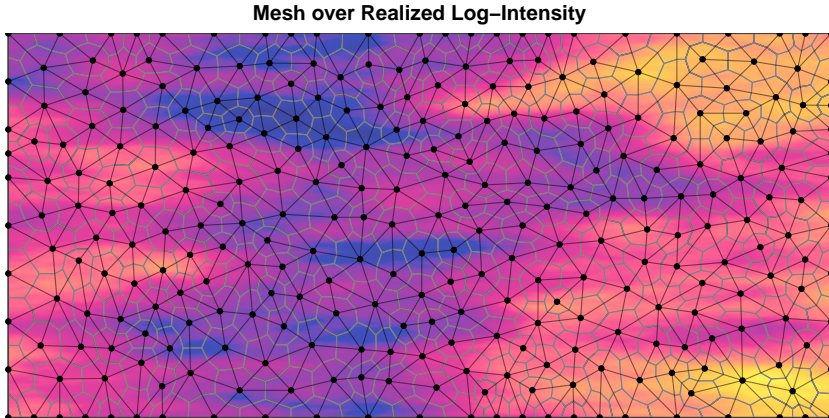


Figure 3: Illustration of the mesh used to approximate the latent GP. The mesh nodes are used in a numerical integration scheme where they are weighted by the area of their dual cells (outlined in grey).

relative to the number of observed events, making the mesh the primary driver of computational complexity in fitting the model.

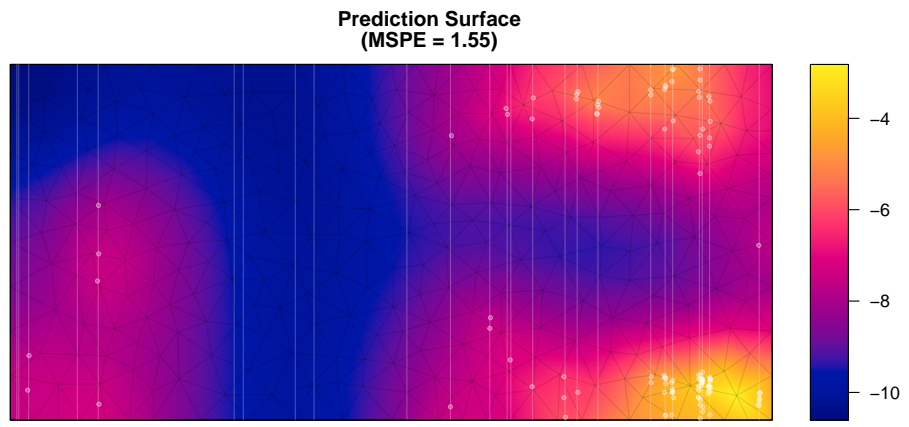
320 A good approach in practice is to refit the model with several meshes and refine the mesh until the prediction surface has converged. However, for a simulation study we must choose one mesh that will perform reasonably well for a wide variety of observations. This mesh is adequately fine to model the large-scale trends in the surface while keeping the computing time well under a minute for each model fit.

325

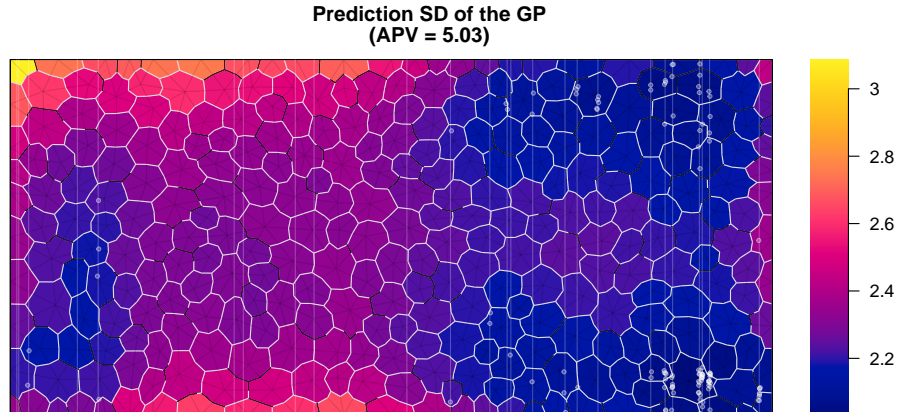
4. Results

In describing the results, we focus on one LGCP dataset and one LGCP with Clusters dataset (Figure 2). The results are similar for all datasets (see figures in Appendix A). These two datasets were chosen for illustration because the simulations using them exhibited a wide variety of outcomes. This included a mix of very good and very poor prediction performance.

330 Figure 4 shows an example where the model does well at predicting the intensity of the realized LGCP from data observed along one of the SRS paths.



(a) Predicted log-intensity



(b) Prediction SD

Figure 4: Predicted log-intensity function and prediction standard deviation using data observed via a SRS of line transects. The SD is shown for each finite element node. This example is a medium-effort plan applied to a LGCP dataset.

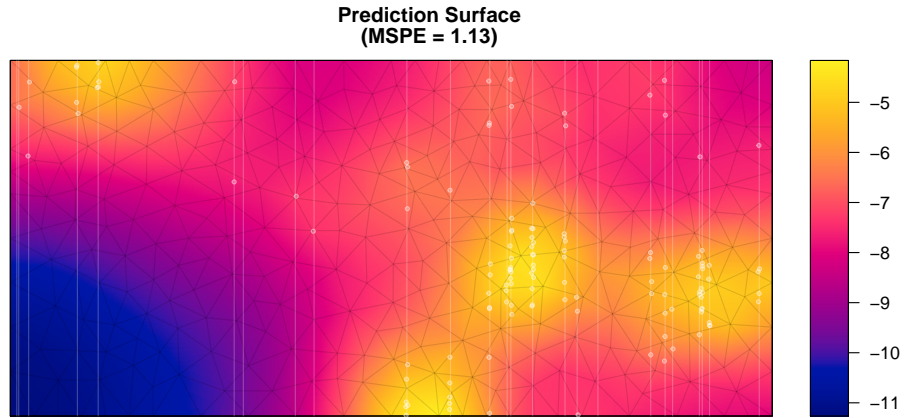
In the figure, the path appears in white and the observed events are shown
335 as white dots. The posterior predicted mean of the log-intensity (top panel)
accurately captures the large-scale features, but smooths out much of the small-
scale variation. The bottom panel shows the prediction standard deviation for
each mesh node. The SD ranges from 2.0 to 3.1, and is lowest near observed
events. SD increases farther from observed events, including in places where the
340 surveyed area was observed to contain no events.

This same survey plan also did well for the LGCP with Clusters dataset, with
the model accurately capturing the large-scale details of the intensity function,
including two of the circular hotspots corresponding to clusters (Figure 5a).
However, it also smoothed the surface quite a bit, notably merging the two
345 overlapping clusters into a single oblong hotspot.

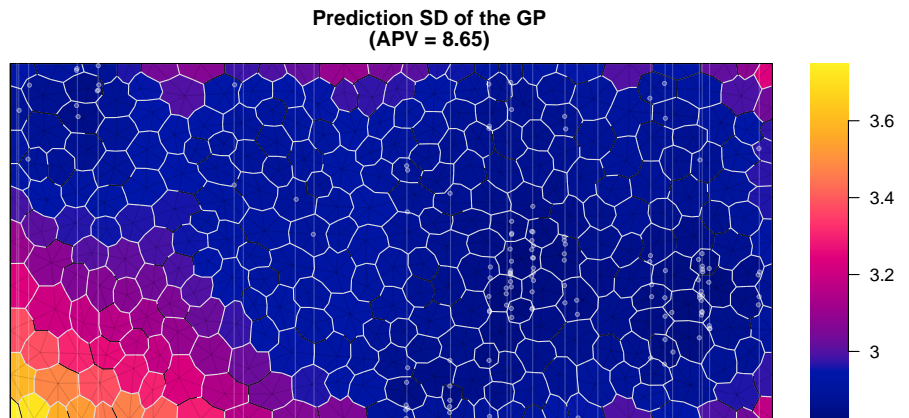
Most plans yielded similar prediction surfaces, capturing the large-scale
trends, and having the least uncertainty near observed events. Results var-
ied in accuracy at the most extreme peaks and valleys of the intensity function
and in overall SD across the study region.

350 However, a small number of model fits failed to converge, and others suffered
from apparent edge effects. For example, Figure 6 shows the prediction surface
resulting from a serpentine transect plan. The predicted log-intensity has a
hotspot of extremely large values in the southeast corner (notice the color scale).
The hotspot is driven by two nodes on the boundary with very large prediction
355 values. Another, less extreme, edge effect is present in the northeast corner.
The surface also contains many circular peaks centered on observed events.
When computational problems occur, they may be fixed by refining the mesh
at additional computational cost. We were not able to use a finer mesh for all
simulations due to computational limitations, but we point out which schemes
360 are robust to these problems (see Tables B.2 and B.3).

Section 4.1 illustrates refitting the model using a refined mesh. The sections
after that compare the schemes in terms of model-based criteria applied to one
realized LGCP dataset and one realized LGCP with Clusters dataset, and then
discuss the results in the context of spatial coverage.

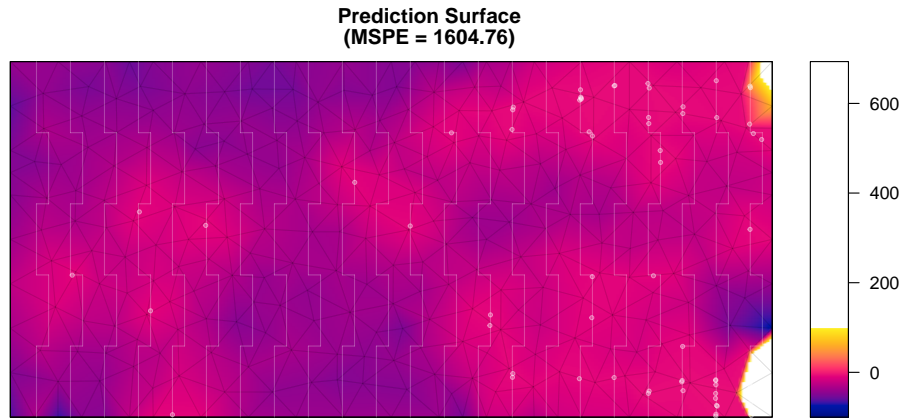


(a) Predicted log-intensity

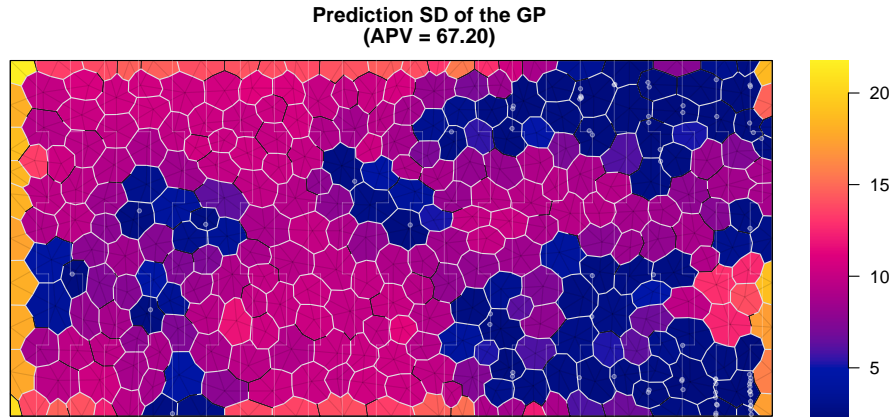


(b) Prediction SD

Figure 5: Predicted log-intensity function and prediction standard deviation using data observed via a SRS of line transects. The SD is shown for each finite element node. This example is a medium-effort plan applied to a LGCP with Clusters dataset.

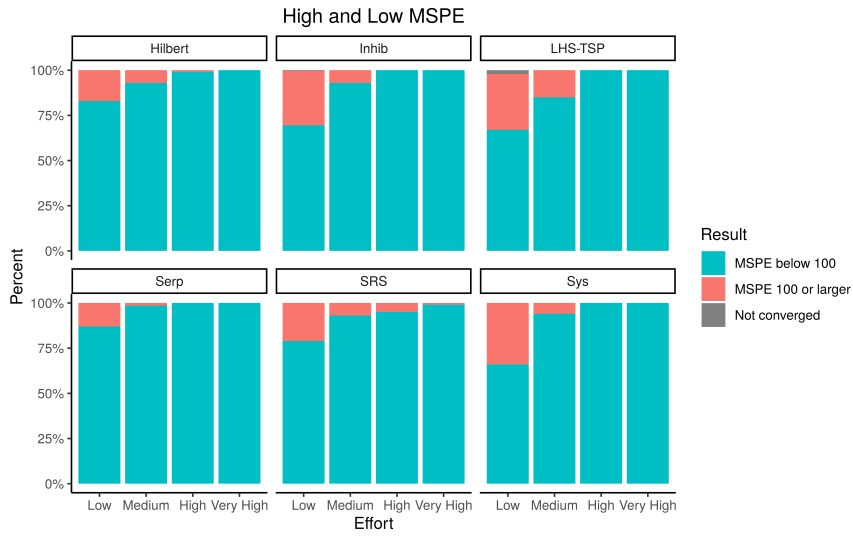


(a) Predicted log-intensity. The color scale is truncated at 100, but reaches a maximum of 692.

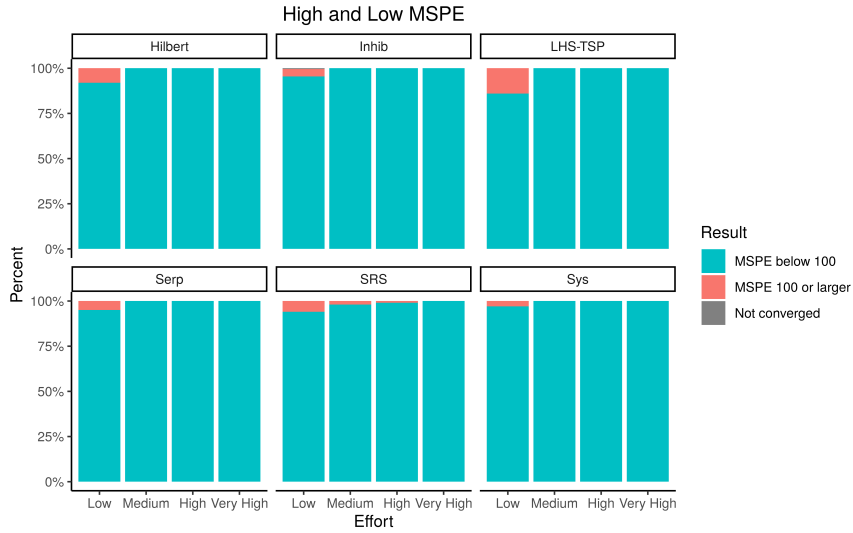


(b) Prediction SD

Figure 6: Predicted GP surface and prediction SD using data observed via a serpentine transect plan. The prediction has an apparent edge effect in the southeastern corner. The SD is high across much of the site. This example is a medium-effort plan applied to a LGCP dataset.



(a) MSPE distribution for one LGCP dataset



(b) MSPE distribution for one LGCP with Clusters dataset

Figure 7: Plots of the distribution of high and low mean squared prediction error (MSPE) vs survey effort for each plan applied to one realization of a LGCP and one realization of a LGCP with Clusters.

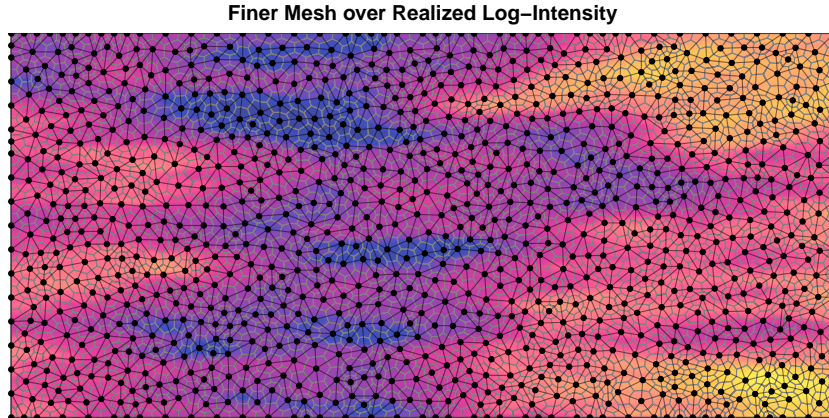


Figure 8: Illustration of a finer mesh than the one used in the full simulation. The mesh nodes are used in a numerical integration scheme where they are weighted by the area of their dual cells (outlined in grey).

³⁶⁵ *4.1. Dealing with computational problems*

A notable proportion of simulation runs resulted in surfaces with edge effects similar to Figure 6, especially at lower levels of sampling effort. This is most likely a symptom of the mesh not being able to represent the posterior surface implied by the observed data. In practice, data analysts should fit the model ³⁷⁰ with several different meshes to assess adequacy of the approximation.

We constructed a finer mesh with 1102 nodes (Figure 8), then refit the model to the point pattern from Figure 6. The resulting log-intensity surface appears in Figure 9. The surface is free of edge effects or extreme values, has an MSPE of 2.31 (down from 1605), and looks generally like well-performing surfaces from ³⁷⁵ other simulation runs using the same dataset (e.g. Figure 4, more examples in the appendix).

This refined mesh has nearly four times as many nodes and the mesh used for the full set of simulations, and consequently fitting the model takes several times longer. The time requirement precluded us from rerunning the full simulation ³⁸⁰ study with this mesh, but the simulations using the coarse mesh provide helpful insight into which schemes are more likely to require more computation effort.

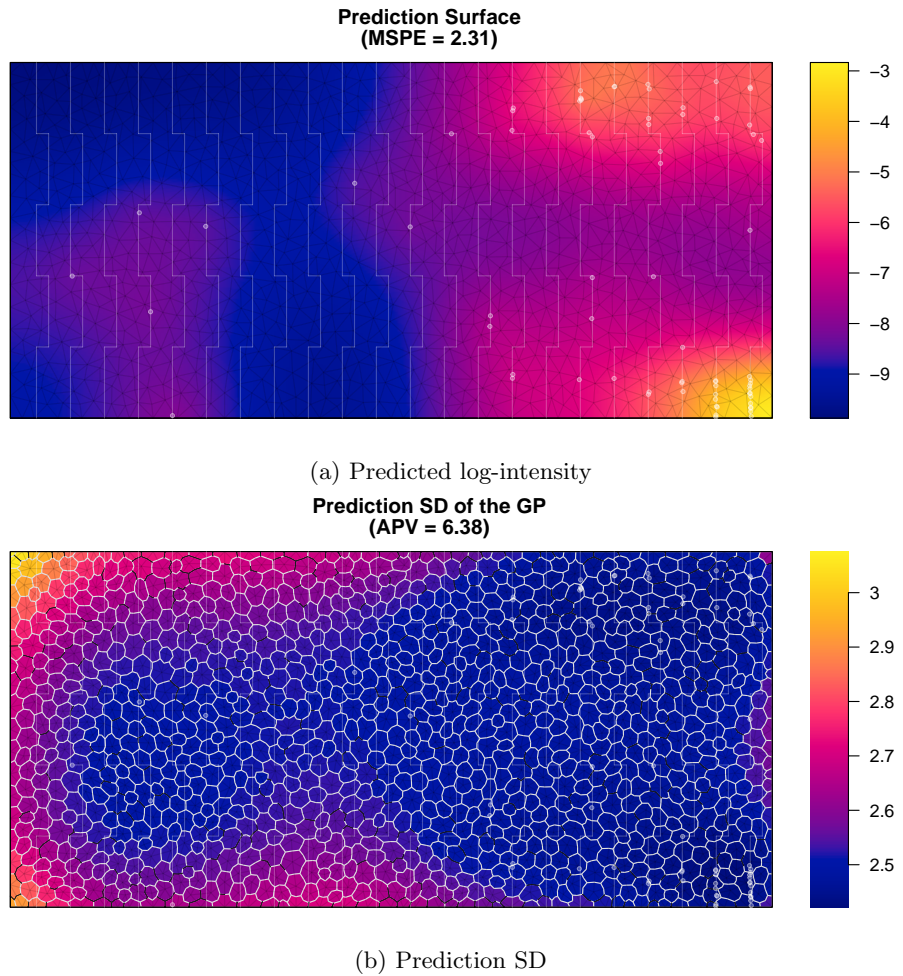


Figure 9: Predicted GP surface and prediction SD using data observed via a serpentine transect plan. The prediction has an apparent edge effect in the southeastern corner. The SD is high across much of the site. This example is a medium-effort plan applied to a LGCP dataset.

4.2. LGCP simulation results

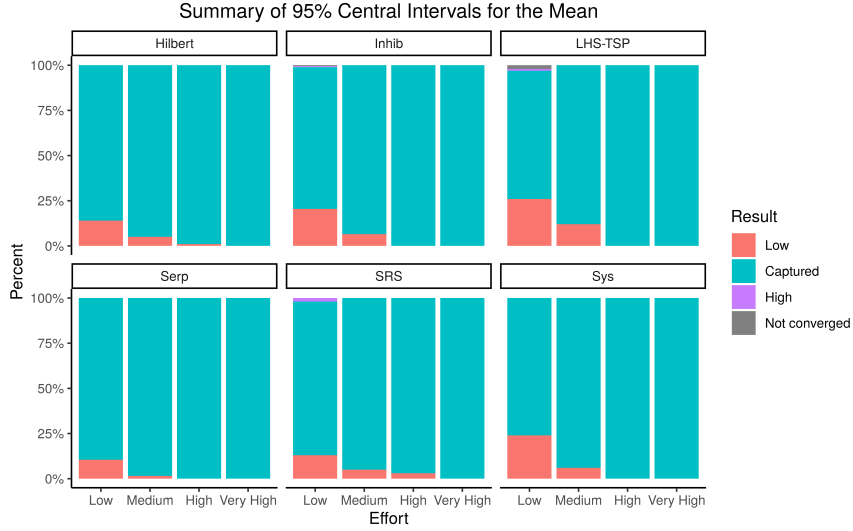
Considered across all survey plans applied to one LGCP dataset, most 95% posterior intervals capture the true mean value, but those that did not were more likely to underestimate than overestimate the mean (Figure 10a). The capture rate increases with survey effort, with only the SRS and Hilbert schemes being observed to miss the true mean at the hight effort level.

Both MSPE and APV had right-skewed distributions. Thus we use logarithmic scales for plots and summarize them using the median and interquartile range (IQR). Median MSPE decreases with increasing path distance, leveling off around between the medium and high effort levels (Figure 11a). Variability (IQR) of MSPE also decreases as effort increases. Prediction surfaces with edge effects form a cluster of large, outlying MSPE values. At all levels of effort, systematic designs had the least variability in MSPE. The lowest-MSPE prediction surfaces result from the longest Hilbert designs, but the distributions of MSPE are similar for all schemes at the high and very effort levels. Overall, the differences among the different schemes with respect to median MSPE are much less than the variability in MSPE within each effort level. The results are largely the same for APV (Figure 11b).

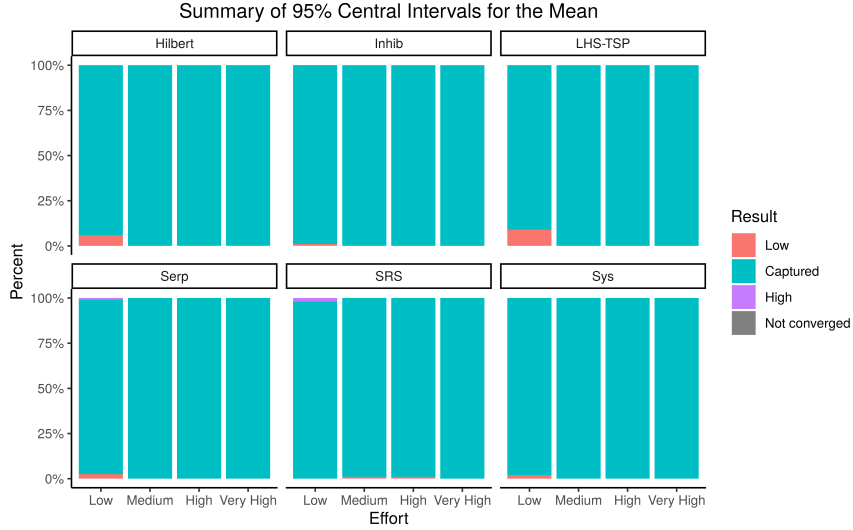
4.3. LGCP with Clusters simulation results

For the LGCP with Clusters dataset, all schemes tended to do well at estimating the mean (Figure 10b). At low effort, all schemes occasionally fail to capture the true mean in a 95% central posterior interval. Only the SRS scheme is observed to miss the mean at medium or high effort.

MSPE and APV again had right-skewed distributions. Median MSPE decreases as effort increases (Figure 12a). Variability in MSPE is roughly constant across effort levels. The systematic scheme had the lowest median MSPE for low and medium effort and low IQR for all effort levels, while the serpentine and Hilbert schemes have the lowest median at high and very high effort. However, differences between schemes are much less than differences across survey effort.

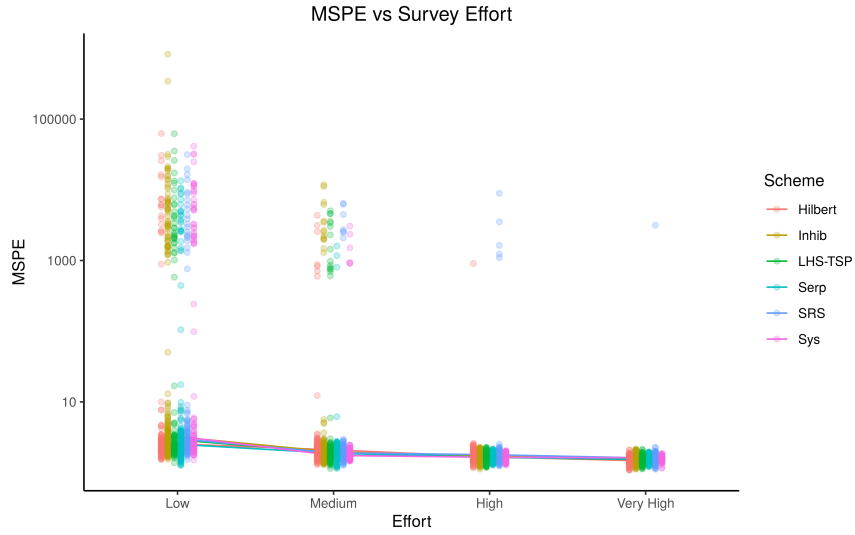


(a) Comparisons of posterior intervals for the intercept to the true mean for one LGCP dataset

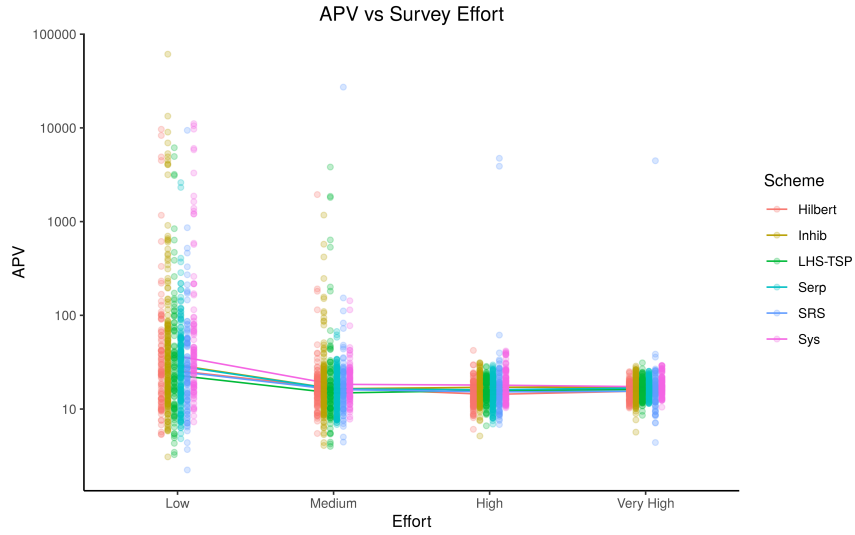


(b) Comparisons of posterior intervals for the intercept to the true mean for one LGCP with Clusters dataset

Figure 10: Plots summarizing comparisons between central 95% posterior intervals for the intercept and the true mean log-intensity of the realized GP. “Captured” indicates that the true mean is inside the interval. “High” and “Low” indicate that the entire interval is, respectively, above or below the true mean.



(a) MSPE vs survey effort for one LGCP dataset



(b) APV vs survey effort for one LGCP dataset

Figure 11: Plots of mean squared prediction error (MSPE) and average prediction variance (APV) vs survey effort for each plan applied to one realization of a LGCP. Line segments connect the median at each effort level.

At low effort, the distribution of APV has a long tail. Otherwise there is little difference in distribution of APV across schemes or effort (Figure 12b).

4.4. Spatial coverage

While the above results suggest the choice of design is relatively unimportant and the distance traveled is the main driver of the quality of the spatial predictions, it is important to consider that all of the design schemes ensure the path is distributed across the entire study region. Designs that leave large unexplored voids will not perform as well.

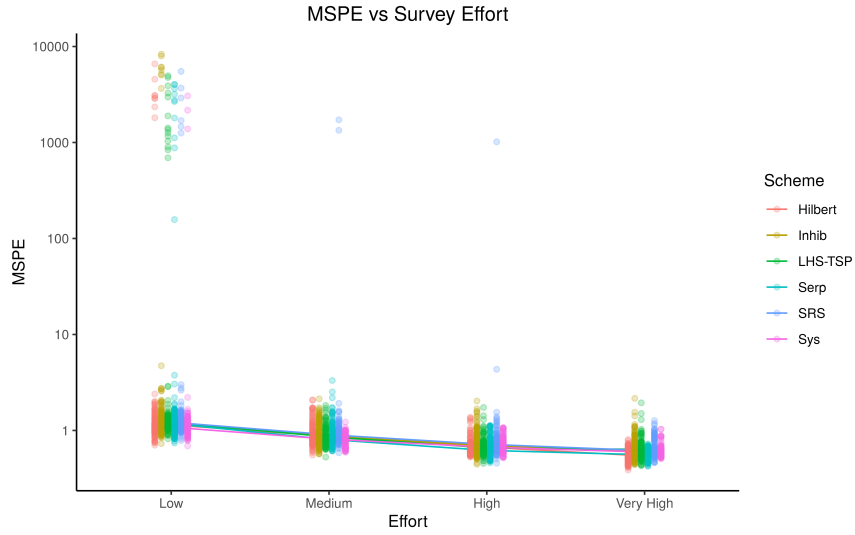
As an example, Figure 13 shows the results of using a systematic sample of 50 parallel transects in the western 20% of the study site. This design is the same length as our high-effort designs, but it leaves most of the site far from the surveyed path. As a result, the predicted log-intensity is flat near the GP posterior mean of -8.71 over most of the site, rendering the prediction mostly useless.

The problem with this example is easily explained in terms of the average distance between the path and arbitrary points in the study site. This example design has an average distance from the path of 486 units; the designs used in the simulation study all had average distances to the path under 130 (with most under 50). In the simulation study, there was little association between MSPE and average distance to the path for paths of comparable length, but the average distance to path decreased as effort (length) increased (Figure 14). This means that all of these schemes do well at distributing the path around the site at all of these effort levels.

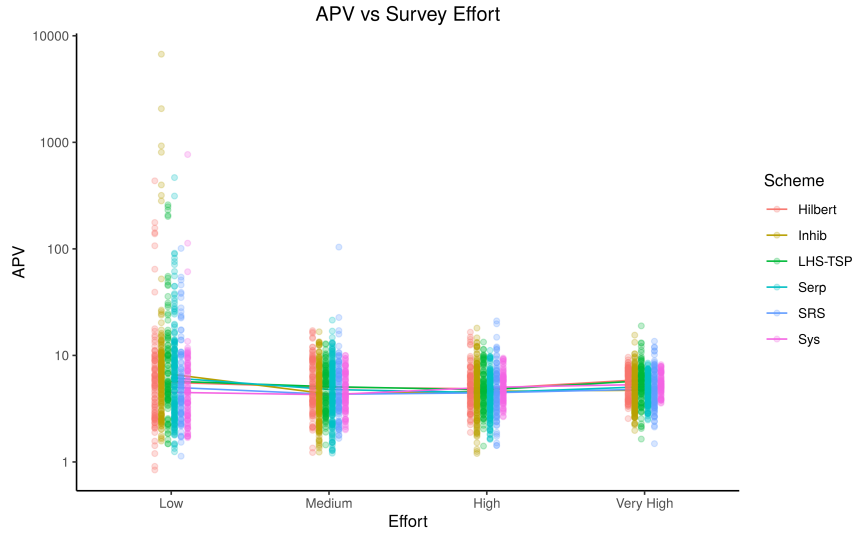
5. Discussion

435 5.1. Implications for sampling

This study provides several insights about optimal sampling for LGCP models. First of all, prediction uncertainty increases with distance from observed events, even along the path (consider the region of low mean and high standard

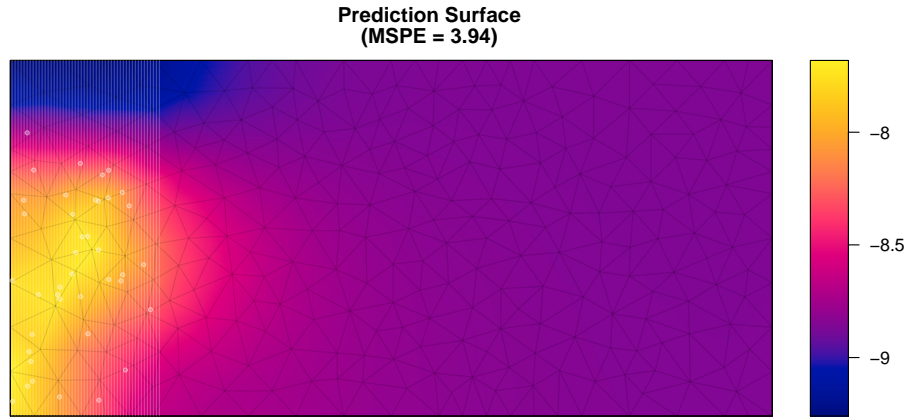


(a) MSPE vs survey effort for one LGCP with Clusters dataset

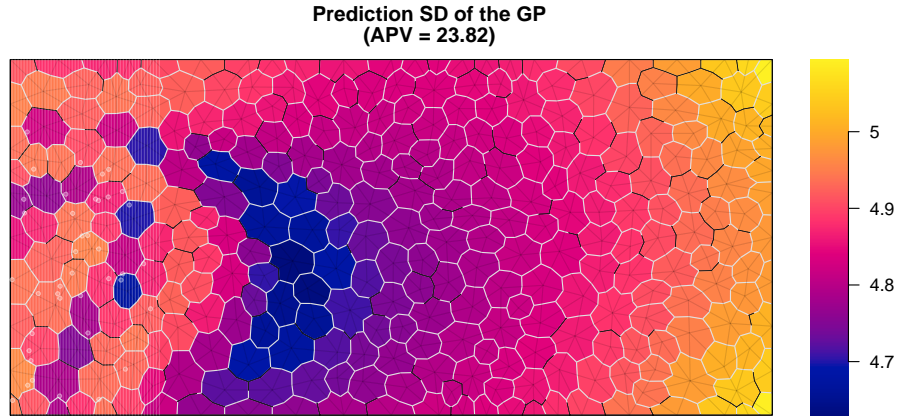


(b) APV vs survey effort for one LGCP with Clusters dataset

Figure 12: Plots of mean squared prediction error (MSPE) and average prediction variance (APV) vs survey effort for each plan applied to one LGCP with Clusters dataset. Line segments connect the median at each effort level.

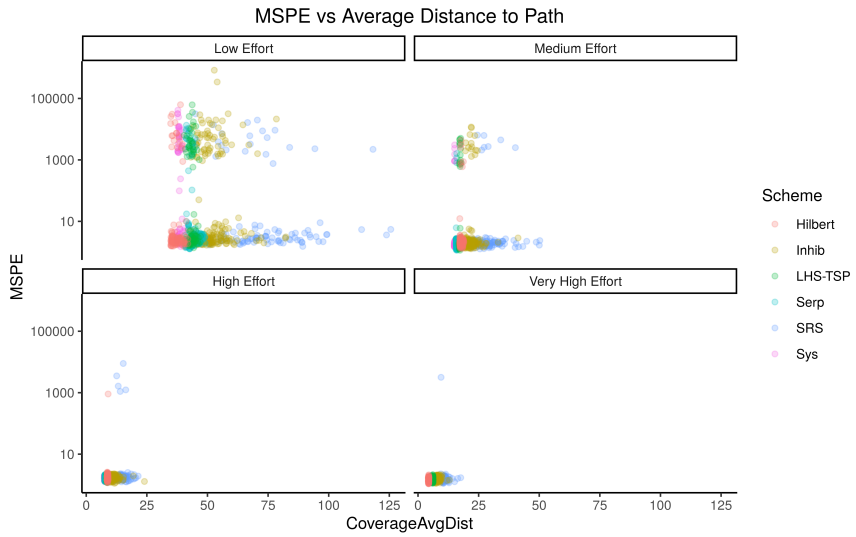


(a) Predicted log-intensity

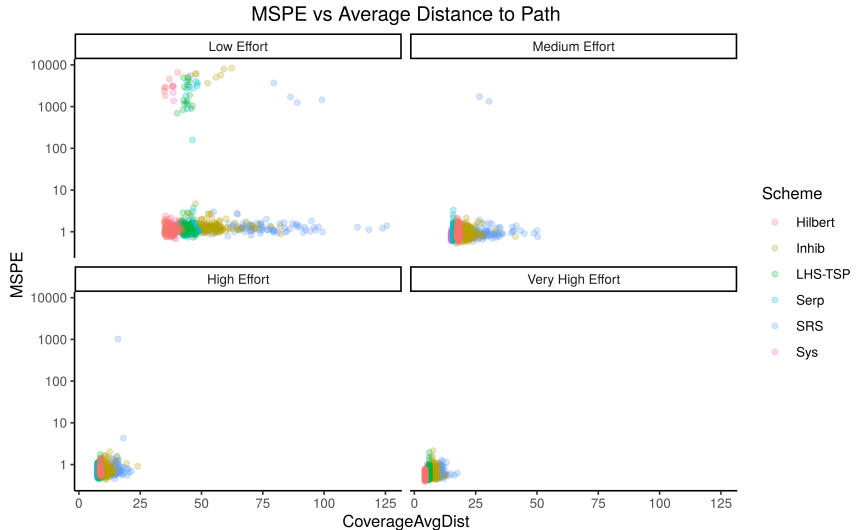


(b) Prediction SD

Figure 13: Predicted log-intensity function and prediction standard deviation using data observed via a systematic sample of a small section of the site. The SD is shown for each finite element node.



(a) MSPE vs coverage for one LGCP dataset



(b) MSPE vs coverage for one LGCP with Clusters dataset

Figure 14: MSPE plotted against the maximum distance from any point in the site to its the nearest point on the path. As survey effort increases, the cloud of points drifts down (lower MSPE) and to the left (lower average distance to the path).

deviation in the southwestern corner of Figure 5b). This behavior is different
440 from the behavior of Gaussian process models in geostatistical studies, where ob-
served design points all provide information that reduces uncertainty of nearby
predictions, regardless of the values observed. In the LGCP model setting, an
”observed” strip that is observed to contain no events does not reduce the uncer-
tainty in nearby predictions. This is reasonable behavior with sparse sampling
445 because there may be events just out of detection range. Intuitively, observing
no events tells us the intensity should be “low” but says little about how low,
especially when intensity is modeled on a logarithmic scale.

This has consequences for adaptive or sequential design. A greedy algo-
rithm based entirely on minimizing variance may excessively sample regions
450 of low intensity, behavior that is unhelpful if the goal is to map hotspots of
high intensity. We recommend including design-based considerations of spatial
coverage in future studies on multi-stage design.

Additional considerations of applying path design to real-world studies in-
clude practical issues of data collection. Generally the path will be smoothed,
455 without the perfectly-straight segments and instantaneous direction changes of
our simulated data collection. Equipment may have limitations which render im-
possible the sharp corners of LHS-TSP designs or the repetitious short segments
and right angles of Hilbert curves. Future optimal design work could incorpo-
rate turn angles into a loss function or use multi-objective optimization (Lark,
460 2016).

5.2. Computing

Bayesian computing (especially INLA) has brought LGCP models into the
realm of practicality. However, this is not yet a fully “push button, get results”
procedure; in a handful of our simulations, the gradient descent step of INLA
465 failed to converge with the default settings. In many other simulations, the
posterior predictions appear numerically unstable at nodes on the boundary.

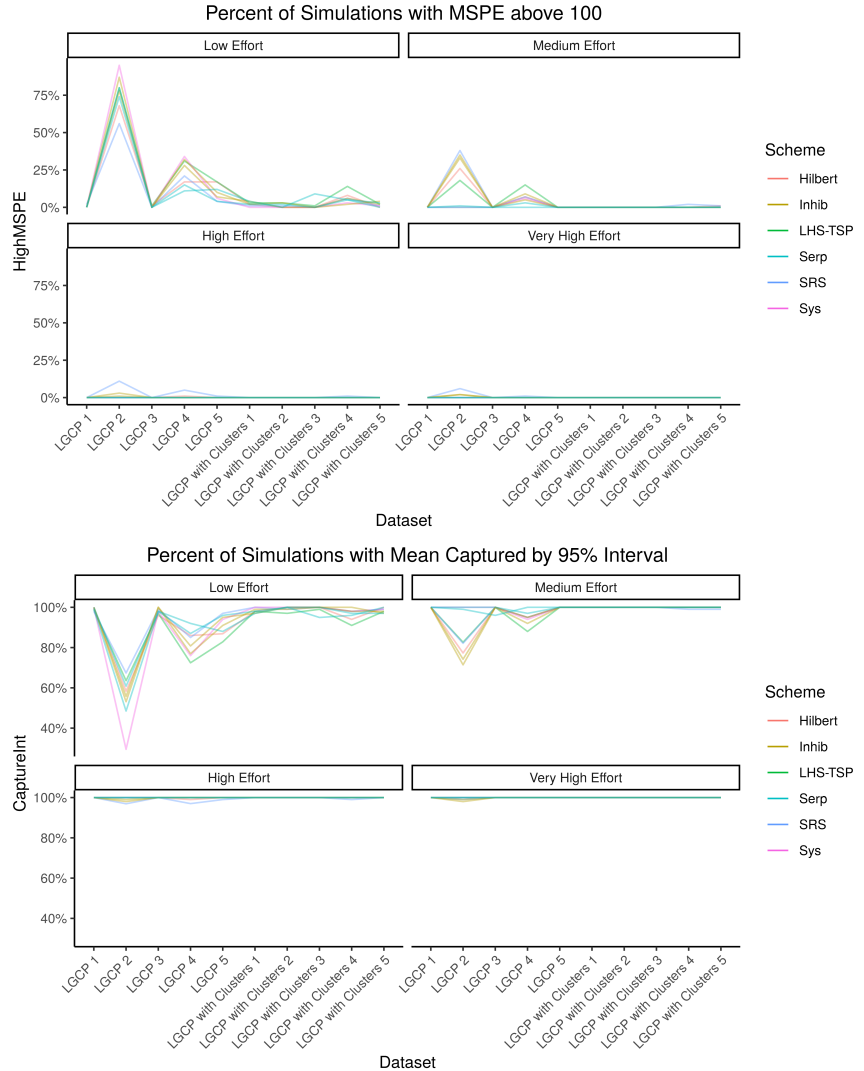
One aspect that would affect both of these issues is the choice of finite
element mesh. A finer mesh than the one used in these simulations would have

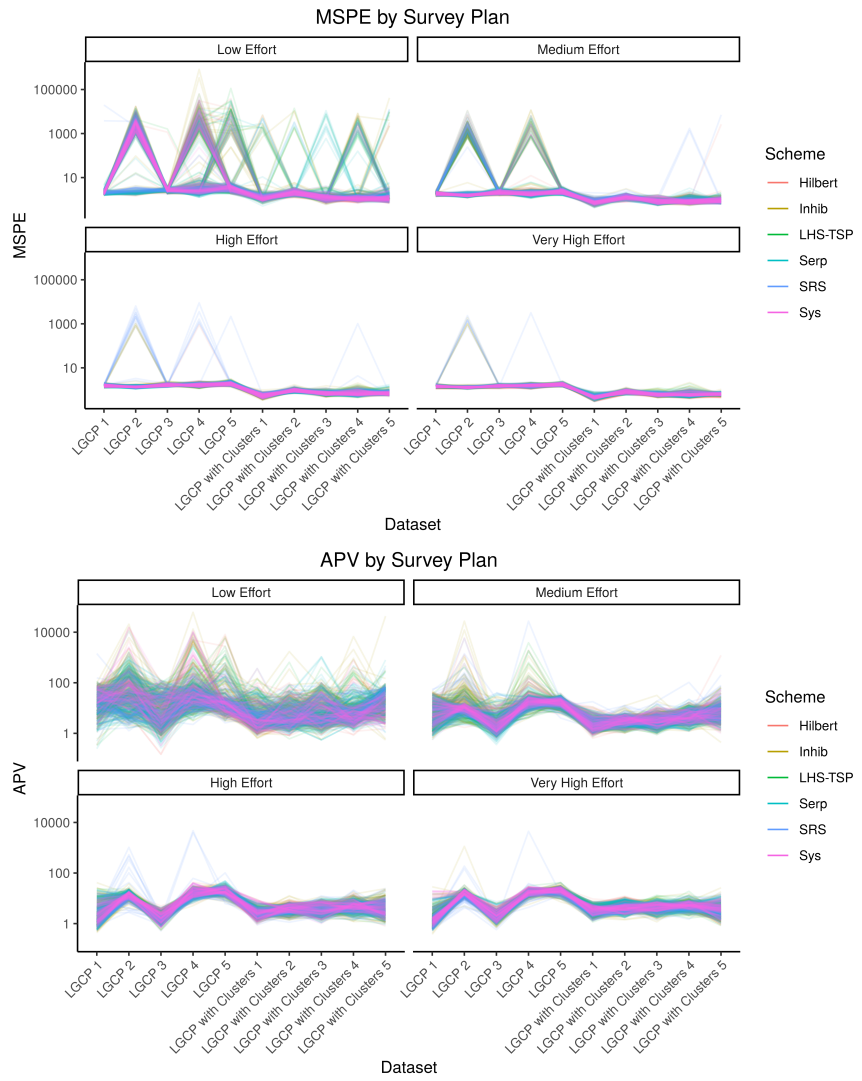
more flexibility to model steep changes in the GP surface. We hypothesize that
470 this would make convergence problems and edge effects less likely. The downside
of a finer mesh is increased computing time because each mesh node becomes
a pseudodata point that must be processed by the model-fitting software. The
choice of mesh is non-trivial and worthy of further study.

5.3. Conclusions

475 For optimal MSPE and APV, the choice of design scheme does not matter
much as long as it provides spatial coverage. For short paths, including corners
and regular spacing help avoid model-fitting problems, as in the Hilbert and
serpentine transect designs. On the other hand, systematic line-transect designs
provide the best spatial coverage but require many transects for good model
480 performance. There is a tradeoff between obtaining a useable posterior and
employing a simple design. We recommend the Hilbert or serpentine designs if
path length is heavily constrained, but systematic line transects are fine if the
path can be long. A simulation using available prior information for a specific
study will be helpful in assessing if a given length is “long enough” to use a
485 line-transect design.

Appendix A. Profiles of designs across all datasets





490

Appendix B. Tables summarizing results

Table B.2: Summary of model fitting and spatial prediction for each design applied to a single LGCP dataset.

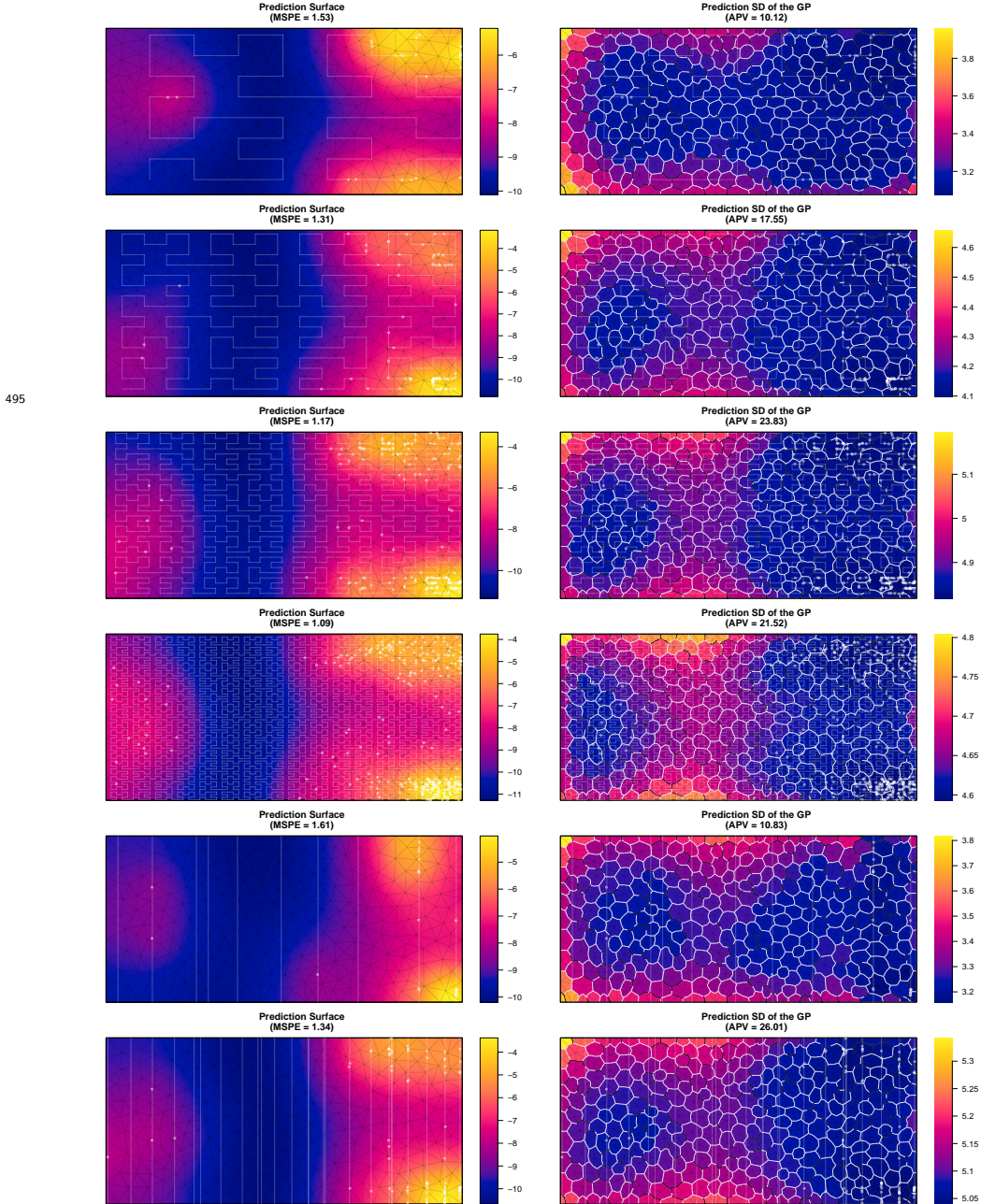
Scheme	Effort	Not Converged	MSPE > 100	Mean Captured	MSPE		APV	
					Median	IQR	Median	IQR
SRS	Low	0%	21%	85%	3.02	3.71	25.2	42.2
	Medium	0%	7%	95%	1.90	0.593	16.2	10.6
	High	0%	5%	97%	1.79	0.442	15.2	7.17
	Very High	0%	1%	100%	1.61	0.399	15.5	4.93
Systematic	Low	0%	34%	76%	3.29	2260	36.8	61.4
	Medium	0%	6%	94%	1.75	0.370	18.4	10.2
	High	0%	0%	100%	1.65	0.216	18.0	11.4
	Very High	0%	0%	100%	1.62	0.158	17.3	5.27
Inhibitory, 10% Close Pairs	Low	0%	32%	77%	3.02	2094	26.9	60.6
	Medium	0%	5%	95%	1.96	0.570	16.7	10.7
	High	0%	0%	100%	1.73	0.367	16.7	5.70
	Very High	0%	0%	100%	1.60	0.345	16.6	5.89
Inhibitory, 20% Close Pairs	Low	1%	28%	80%	3.57	1290	32.2	46.5
	Medium	0%	9%	92%	1.96	0.543	16.4	8.29
	High	0%	0%	100%	1.68	0.382	17.5	5.98
	Very High	0%	0%	100%	1.59	0.289	17.2	5.07
Serpentine, 5 zigzags	Low	0%	11%	92%	2.37	1.33	27.9	35.6
	Medium	0%	3%	97%	1.88	0.350	13.9	9.26
	High	0%	0%	100%	1.64	0.268	14.6	9.27
	Very High	0%	0%	100%	1.55	0.123	16.9	2.87
Serpentine 8 zigzags	Low	0%	15%	87%	2.61	2.07	29.2	33.3
	Medium	0%	0%	100%	1.88	0.408	18.3	8.15
	High	0%	0%	100%	1.64	0.245	17.6	6.25
	Very High	0%	0%	100%	1.53	0.272	16.4	5.41
LHS-TSP	Low	2%	31%	71%	2.90	1777	22.9	57.5
	Medium	0%	15%	88%	1.92	0.730	14.8	14.4
	High	0%	0%	100%	1.64	0.335	15.8	6.80
	Very High	0%	0%	100%	1.53	0.298	16.2	5.61
Hilbert	Low	0%	17%	86%	2.54	1.44	25.6	44.2
	Medium	0%	7%	95%	2.10	0.748	16.7	7.96
	High	0%	1%	99%	1.67	0.438	14.3	5.54
	Very High	0%	0%	100%	1.46	0.388	15.6	4.57

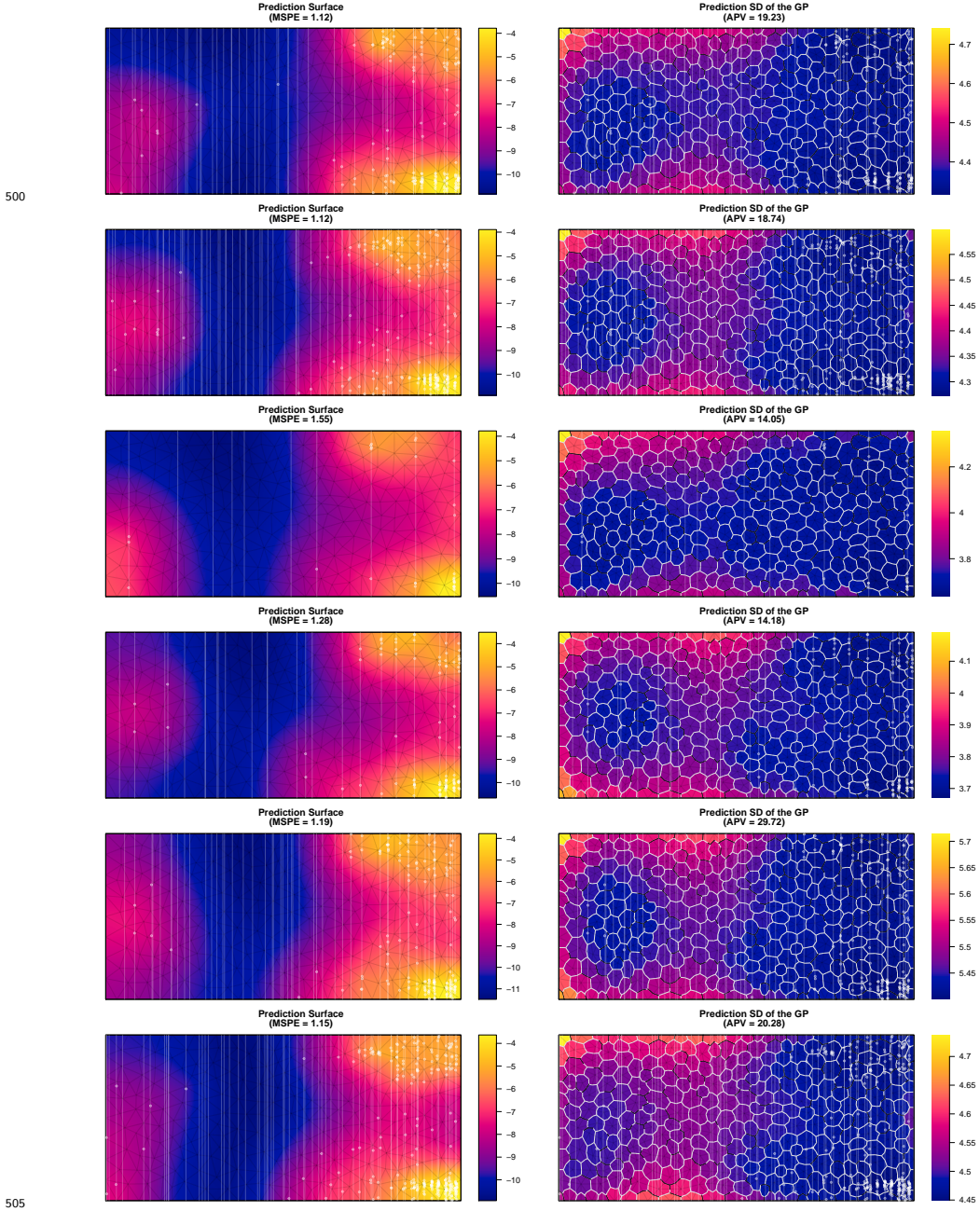
Table B.3: Summary of model fitting and spatial prediction for each design applied to a single LGCP with Clusters dataset.

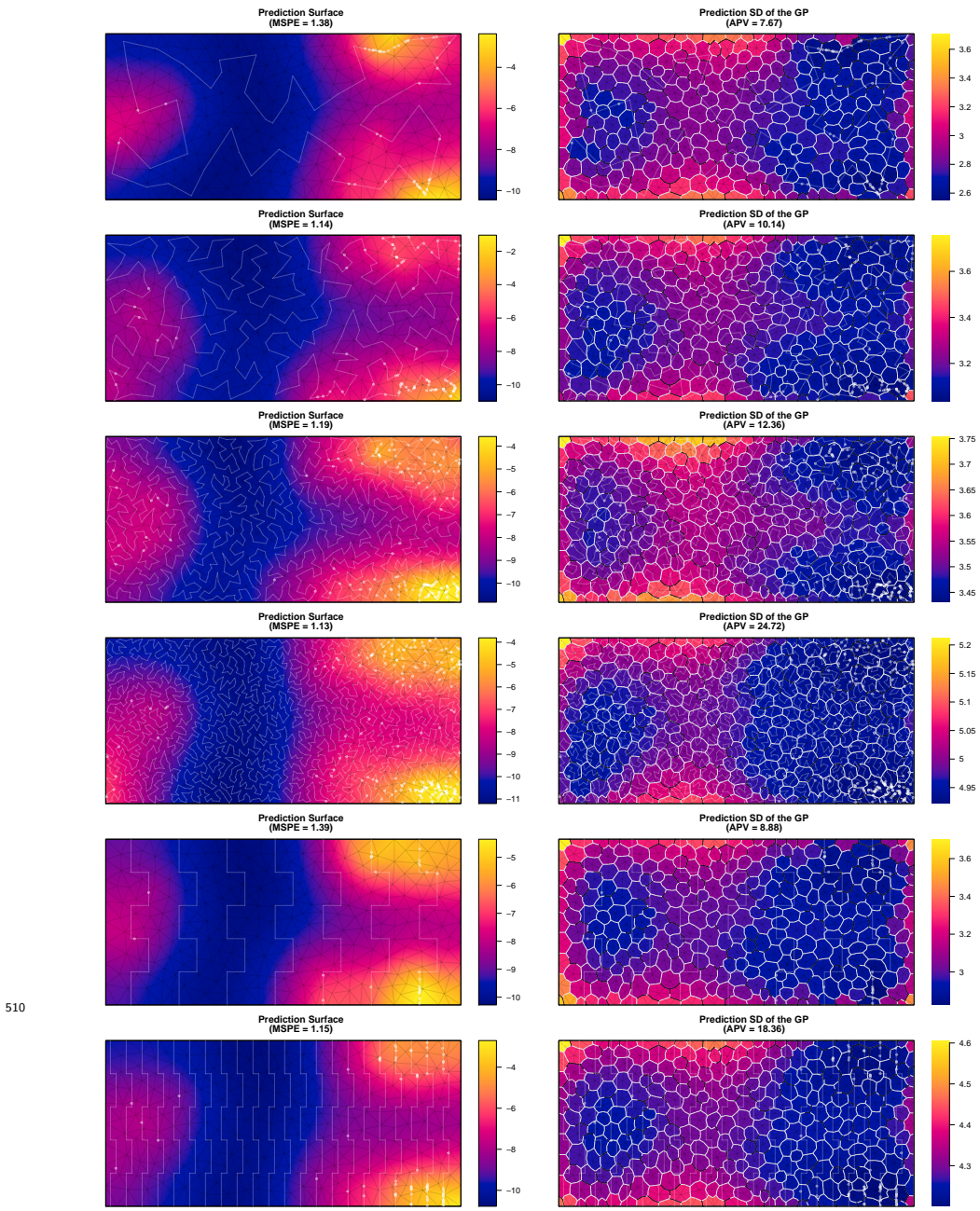
Scheme	Effort	Not Converged	MSPE > 100	Mean Captured	MSPE		APV	
					Median	IQR	Median	IQR
SRS	Low	0%	6%	98%	1.22	0.339	5.02	5.72
	Medium	0%	2%	99%	0.902	0.219	4.32	3.89
	High	0%	1%	99%	0.717	0.216	4.45	3.28
	Very High	0%	0%	100%	0.619	0.223	4.81	2.97
Systematic	Low	0%	3%	98%	1.08	0.338	4.50	4.67
	Medium	0%	0%	100%	0.812	0.199	4.27	2.85
	High	0%	0%	100%	0.671	0.189	5.01	2.02
	Very High	0%	0%	100%	0.596	0.0846	5.33	1.39
Inhibitory, 10% Close Pairs	Low	1%	6%	97%	1.20	0.326	6.93	6.78
	Medium	0%	0%	100%	0.887	0.245	4.92	3.33
	High	0%	0%	100%	0.694	0.167	4.64	2.27
	Very High	0%	0%	100%	0.599	0.144	4.47	2.21
Inhibitory 20% Close Pairs	Low	0%	2%	100%	1.23	0.287	6.42	3.59
	Medium	0%	0%	100%	0.832	0.222	4.19	3.82
	High	0%	0%	100%	0.701	0.253	4.53	3.57
	Very High	0%	0%	100%	0.630	0.204	5.08	2.91
Serpentine, 5 zigzags	Low	0%	5%	96%	1.22	0.364	6.35	8.95
	Medium	0%	0%	100%	0.808	0.259	4.32	4.28
	High	0%	0%	100%	0.597	0.137	4.23	1.73
	Very High	0%	0%	100%	0.530	0.0924	4.32	2.50
Serpentine, 8 zigzags	Low	0%	5%	97%	1.11	0.342	6.10	5.77
	Medium	0%	0%	100%	0.795	0.163	5.14	3.19
	High	0%	0%	100%	0.643	0.235	4.61	2.75
	Very High	0%	0%	100%	0.564	0.0621	5.48	1.65
LHS-TSP	Low	0%	14%	91%	1.21	0.374	5.73	8.92
	Medium	0%	0%	100%	0.858	0.281	5.09	3.81
	High	0%	0%	100%	0.658	0.160	4.75	3.12
	Very High	0%	0%	100%	0.635	0.198	5.79	2.96
Hilbert	Low	0%	8%	94%	1.14	0.451	5.57	6.15
	Medium	0%	0%	100%	0.871	0.358	5.02	5.03
	High	0%	0%	100%	0.669	0.152	4.86	2.64
	Very High	0%	0%	100%	0.542	0.138	5.95	2.82

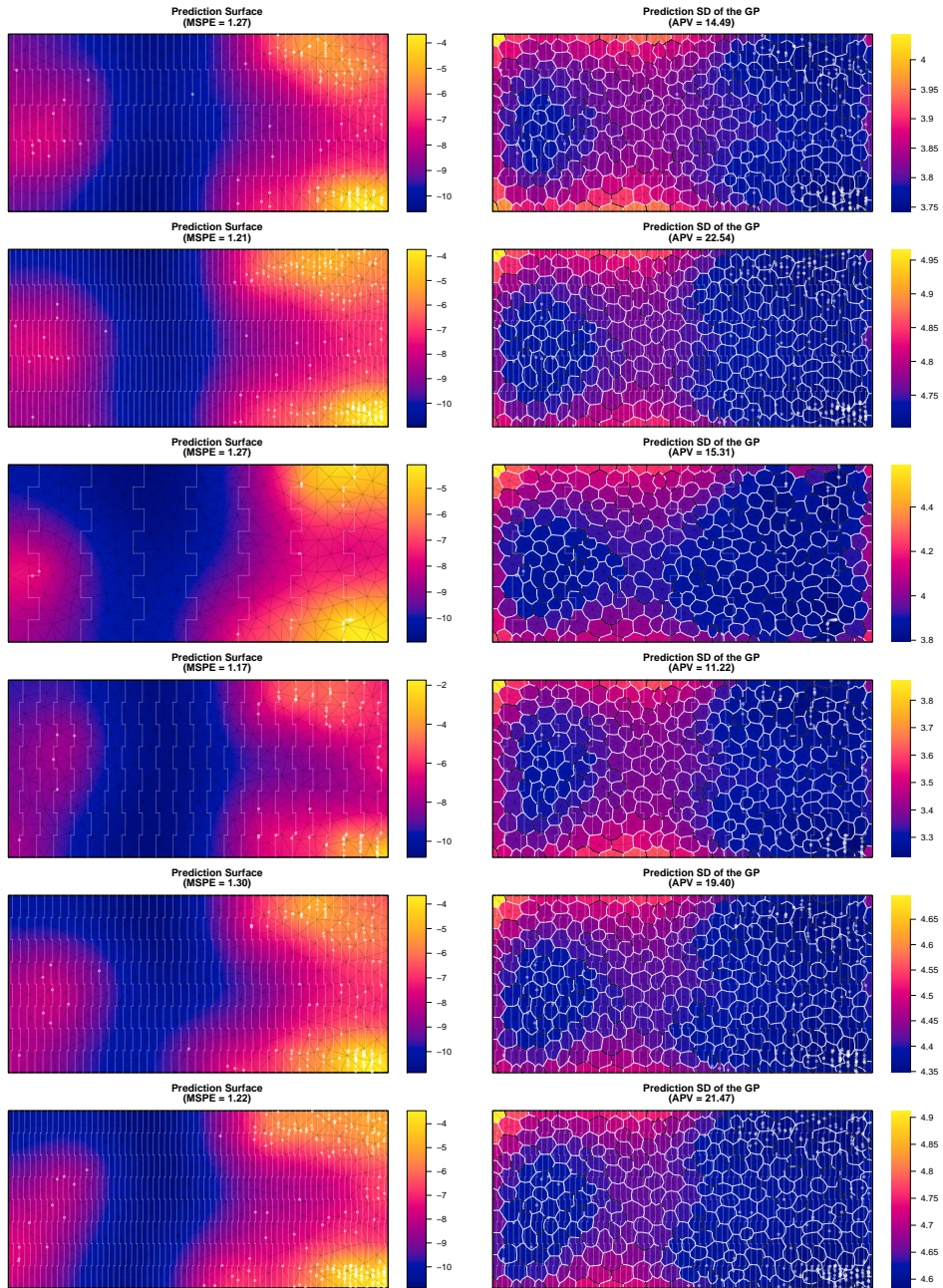
Appendix C. Additional plots of posterior predictions

Appendix C.1. Minimum-MSPE surfaces, LGCP dataset

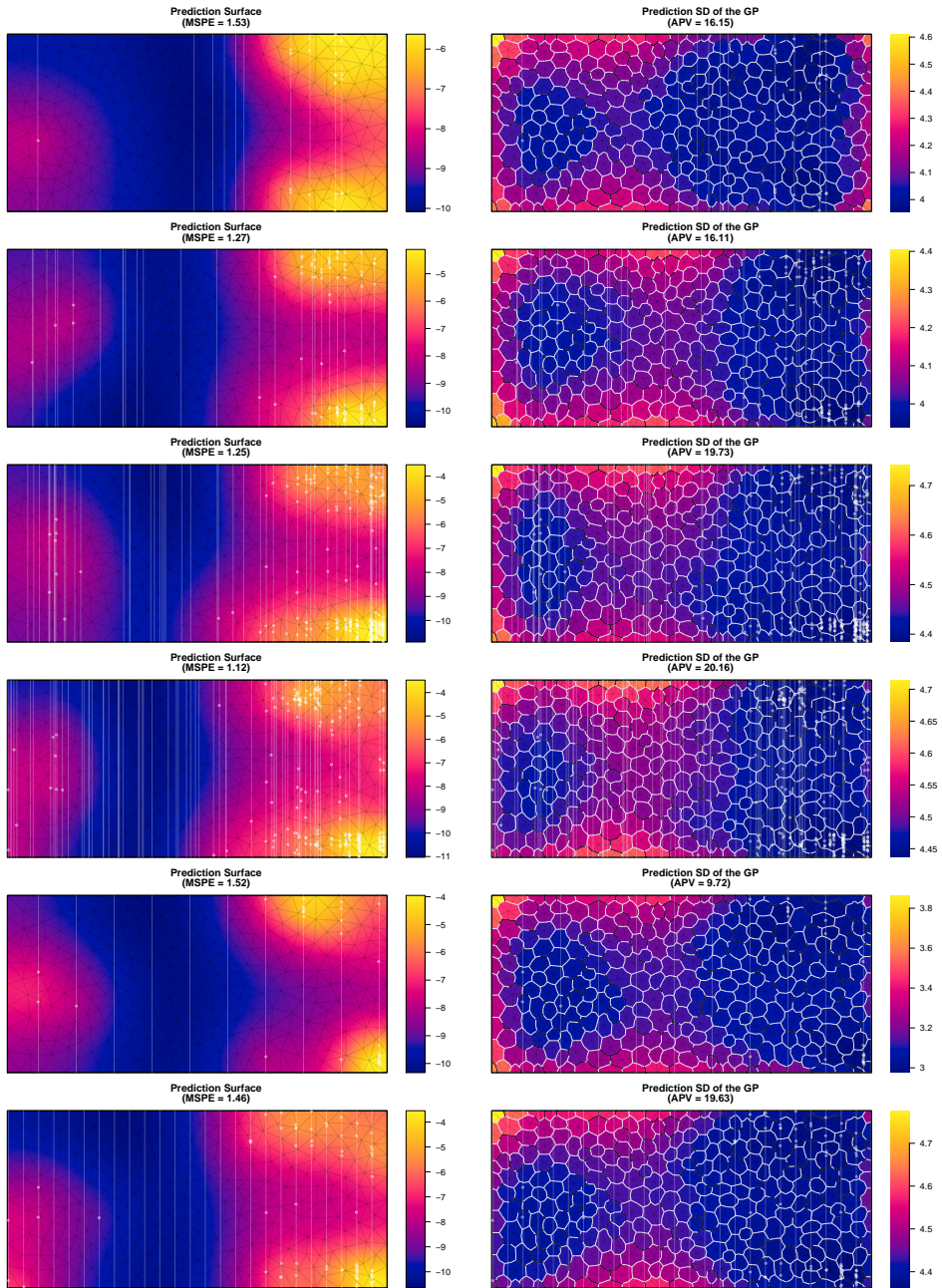


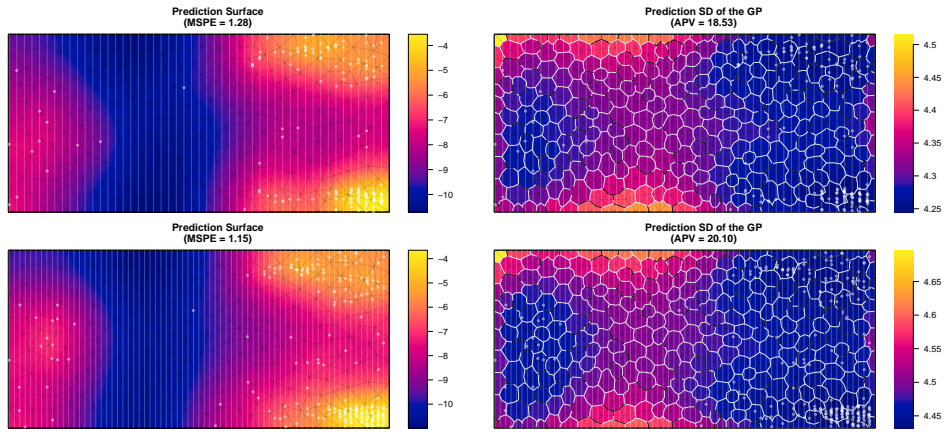




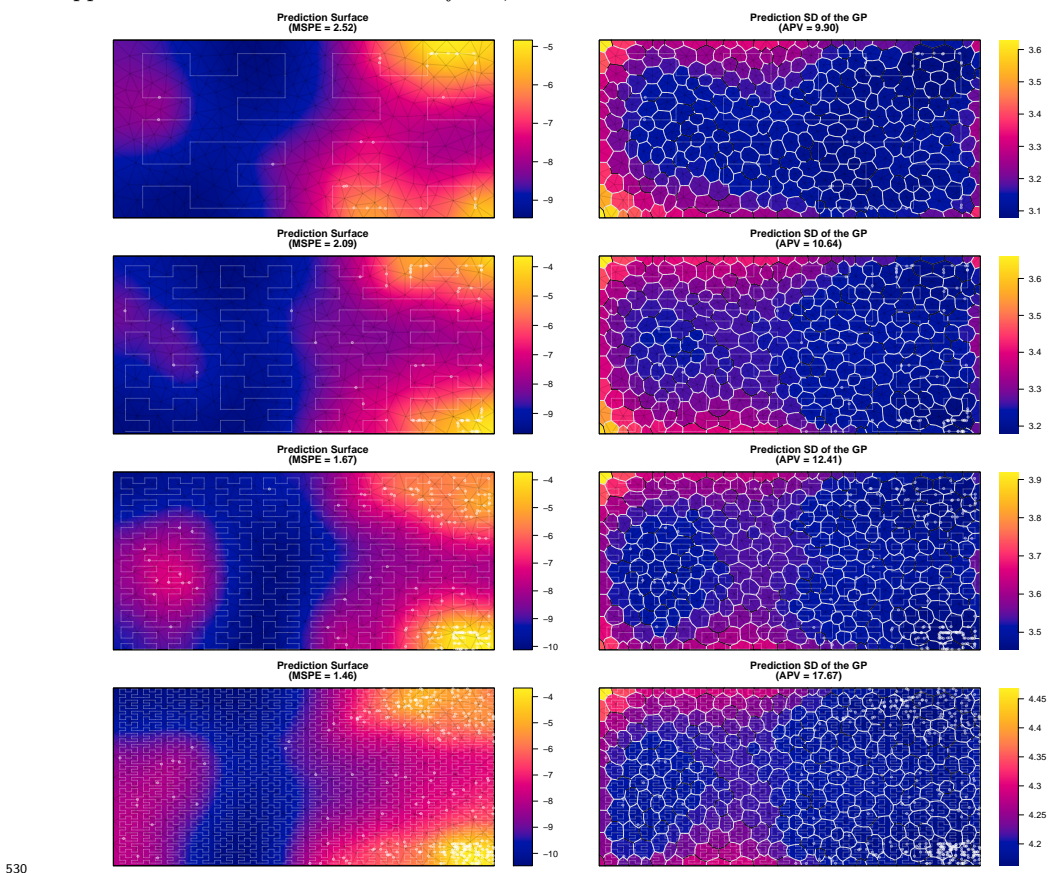


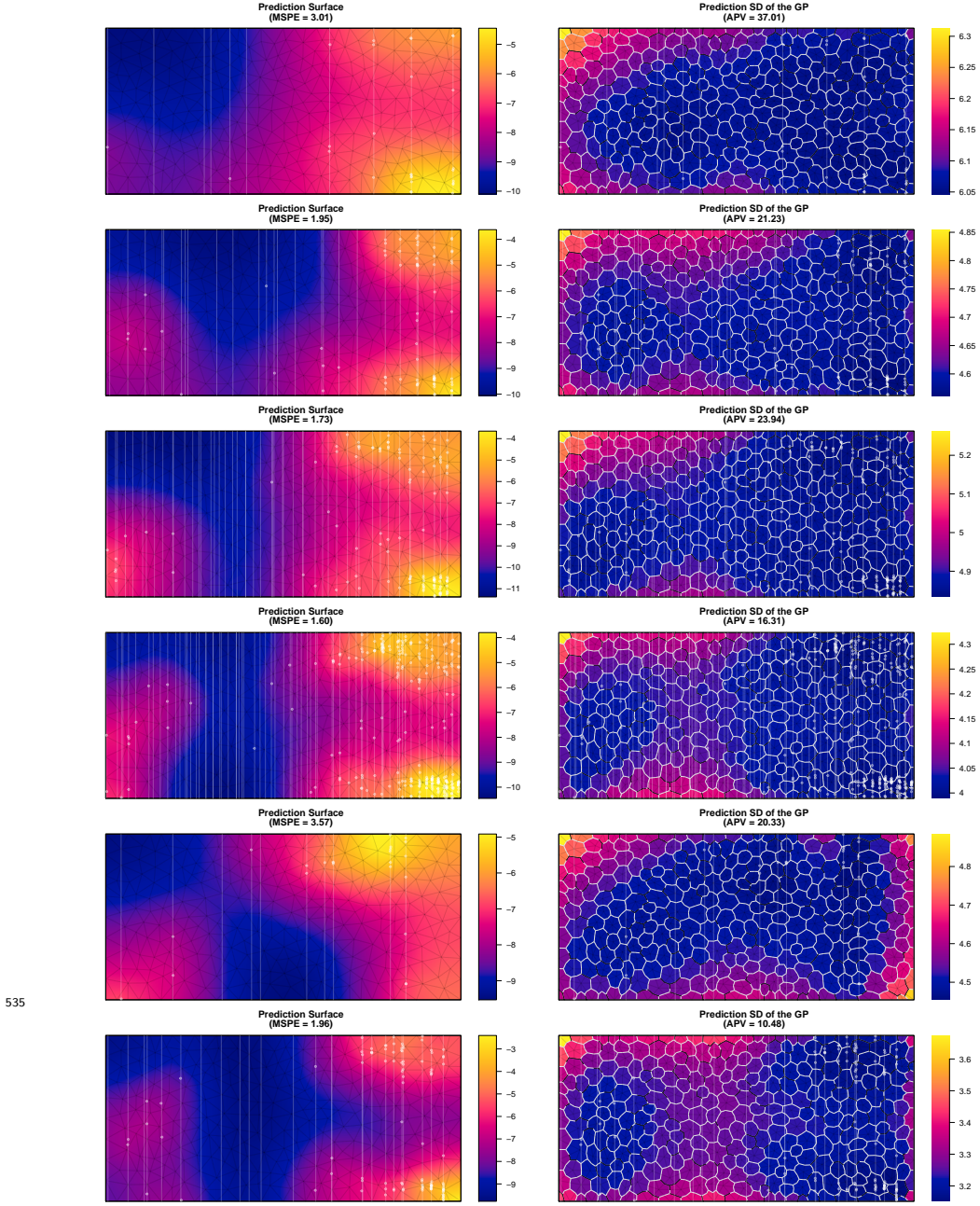
520

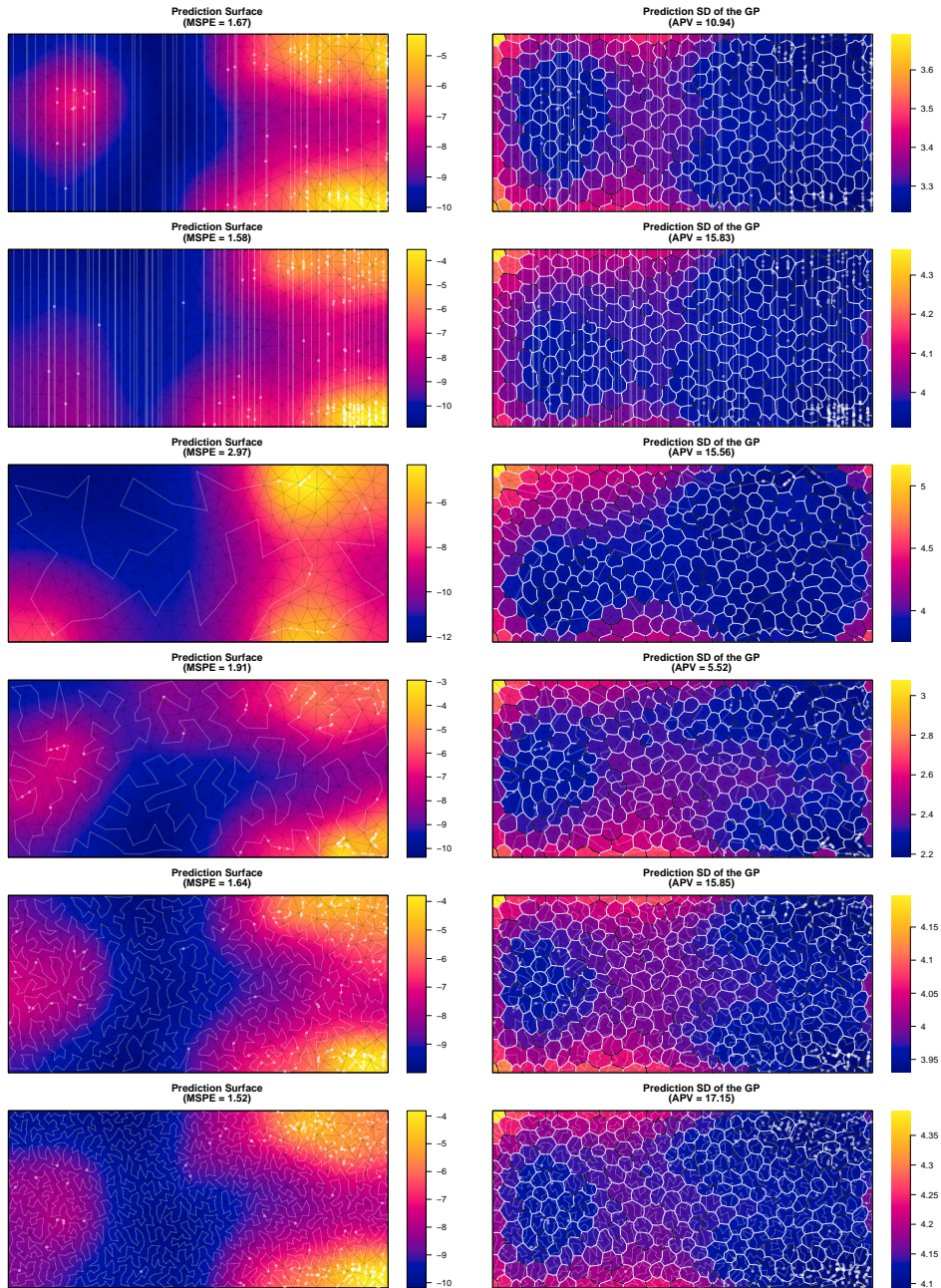


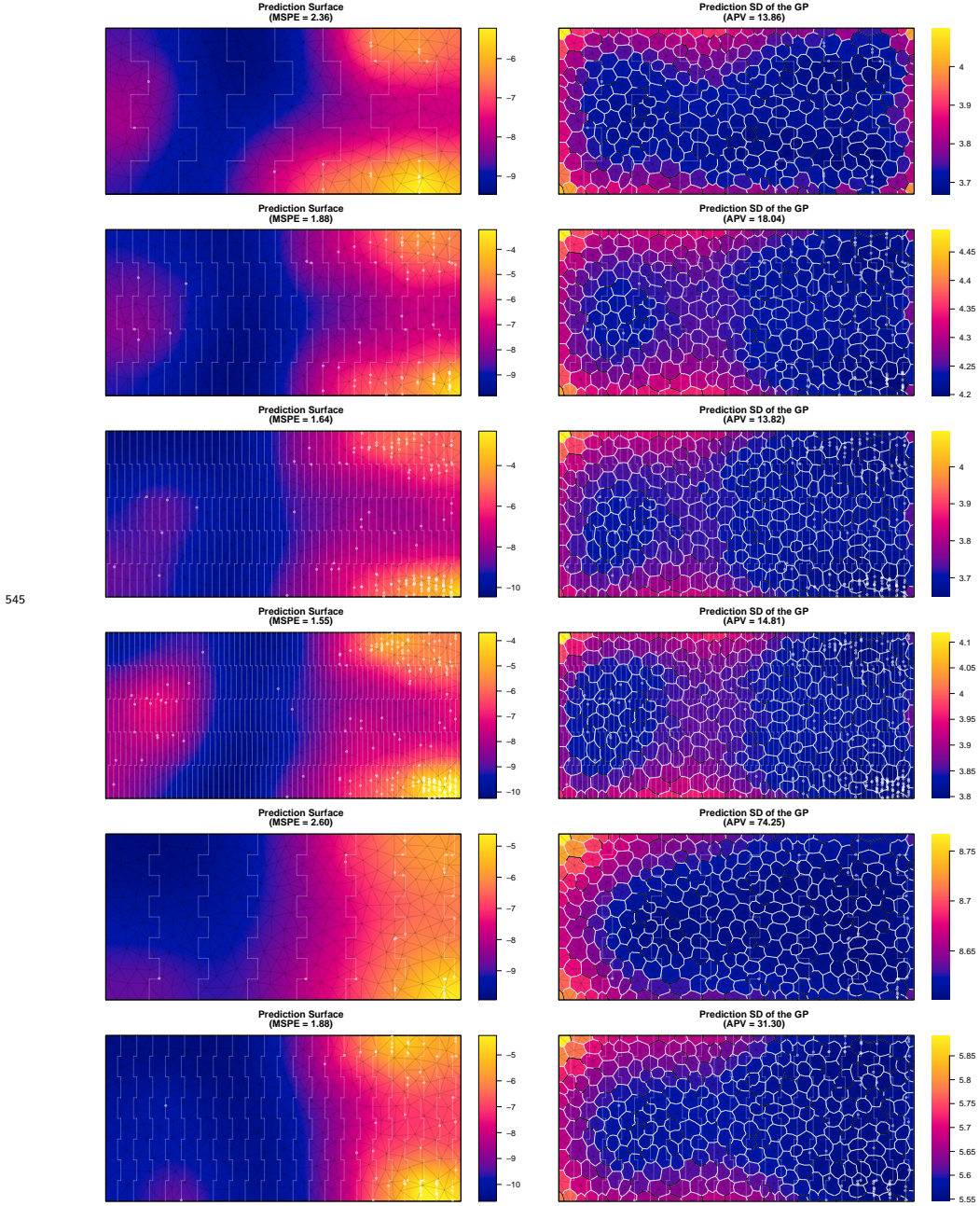


Appendix C.2. Median-MSPE surfaces, LGCP dataset

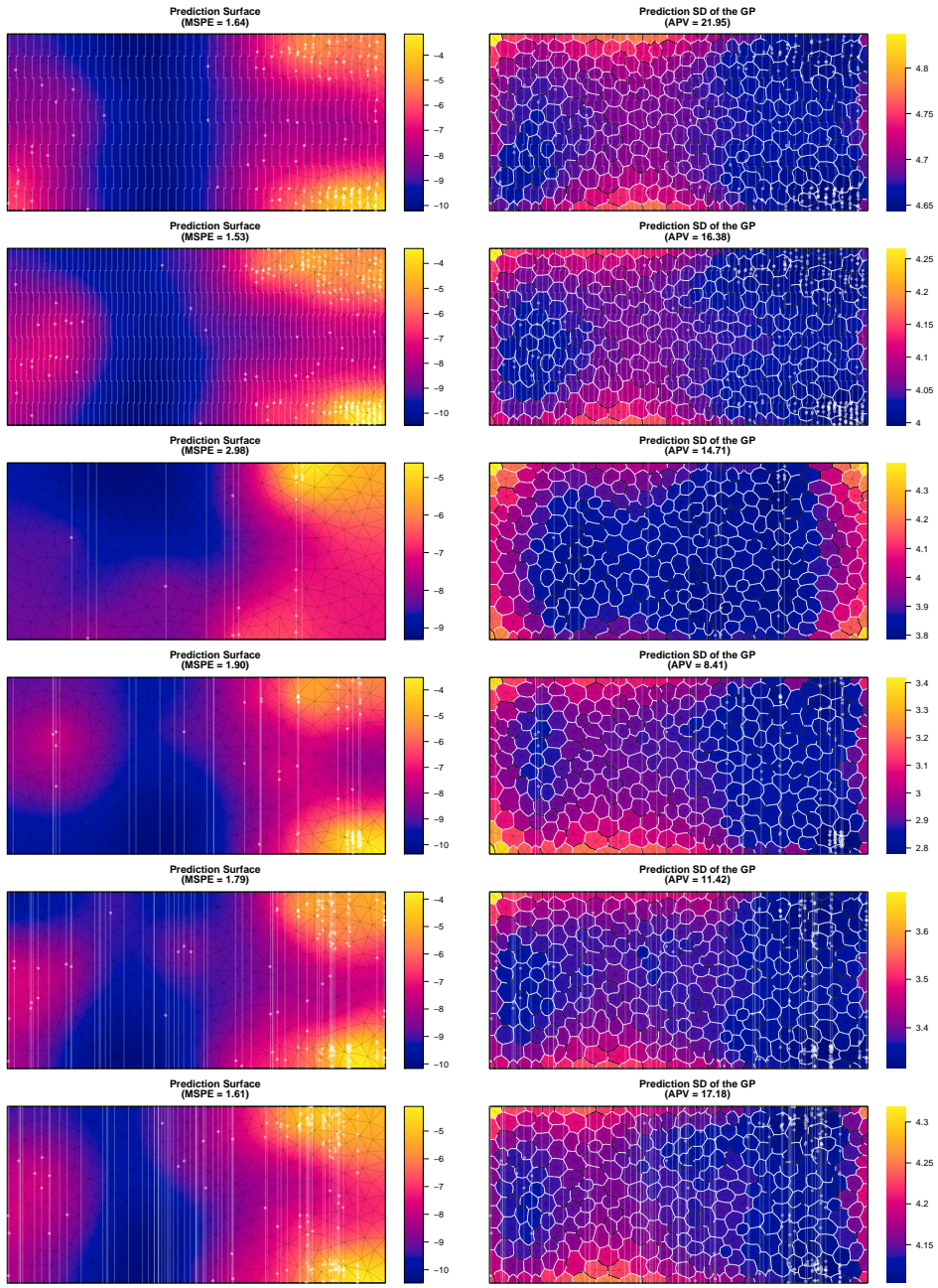


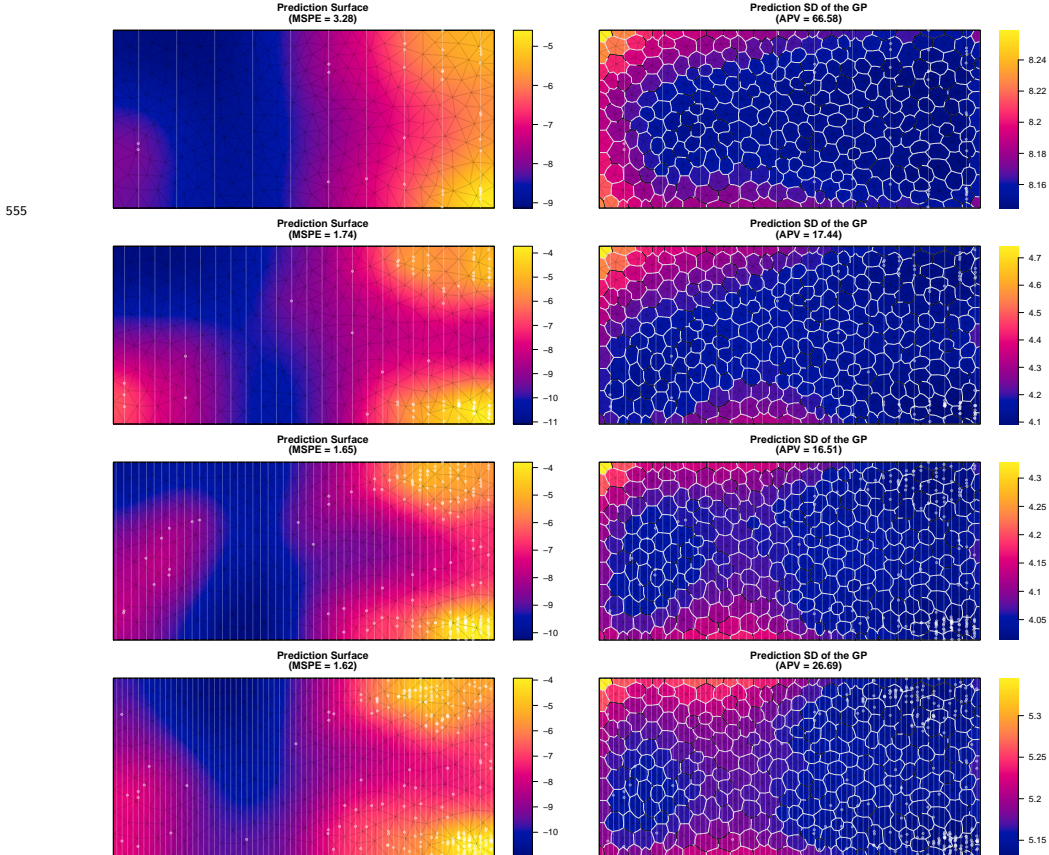




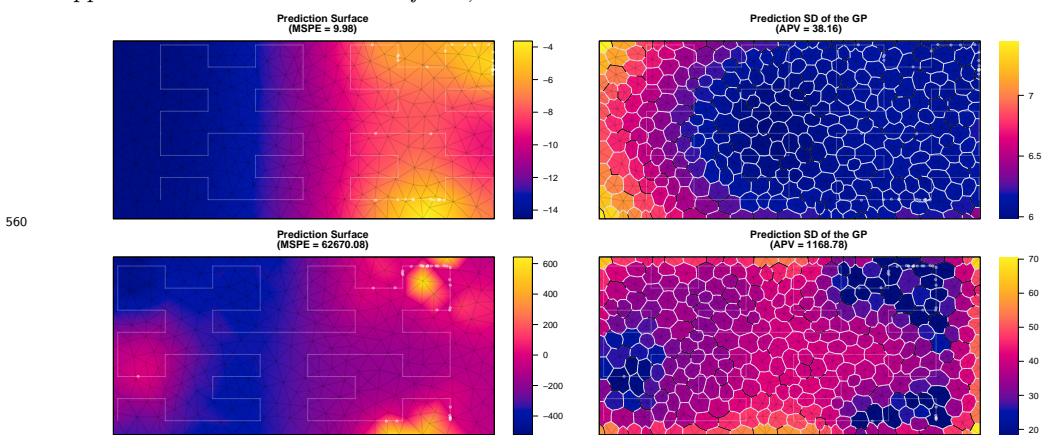


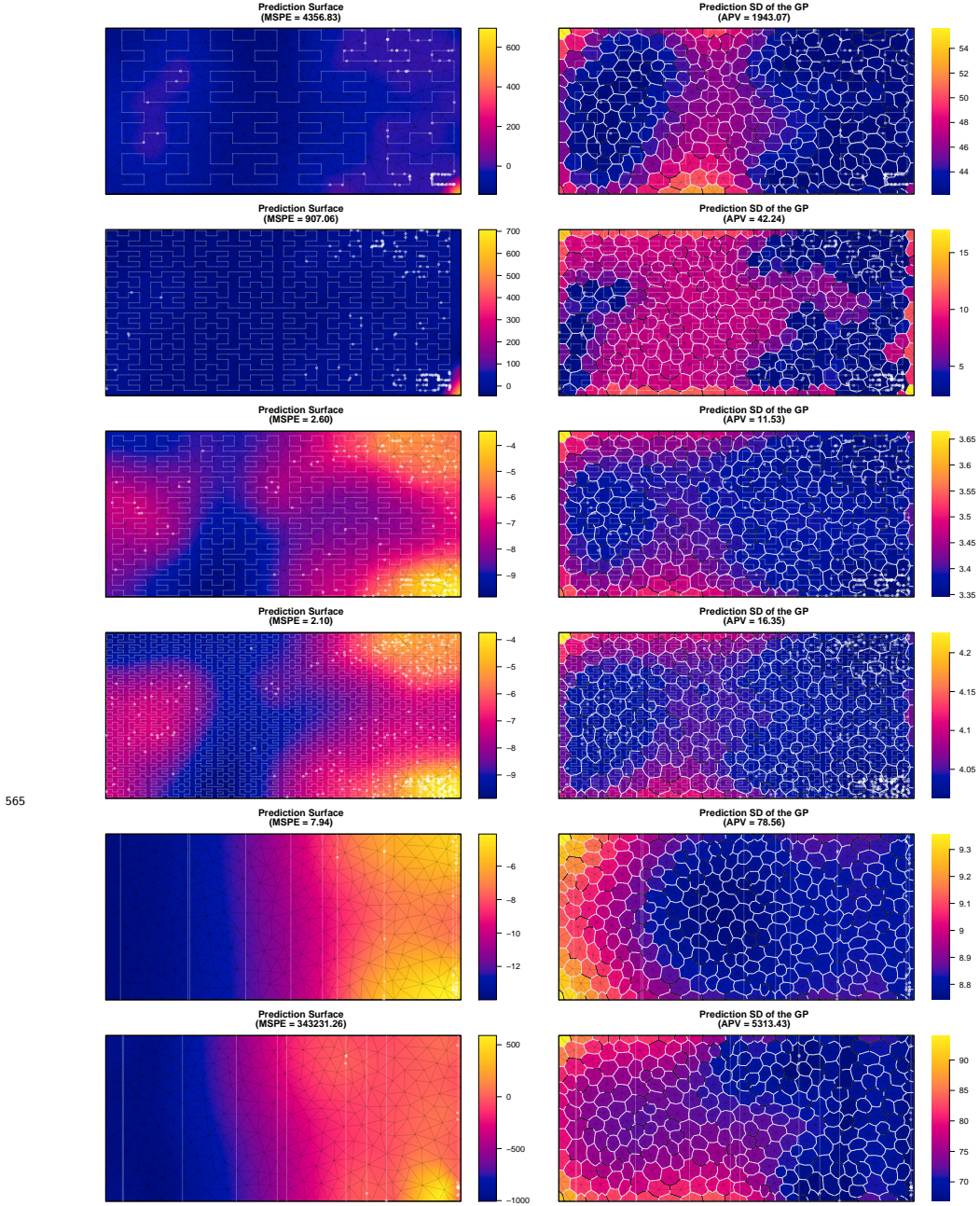
550



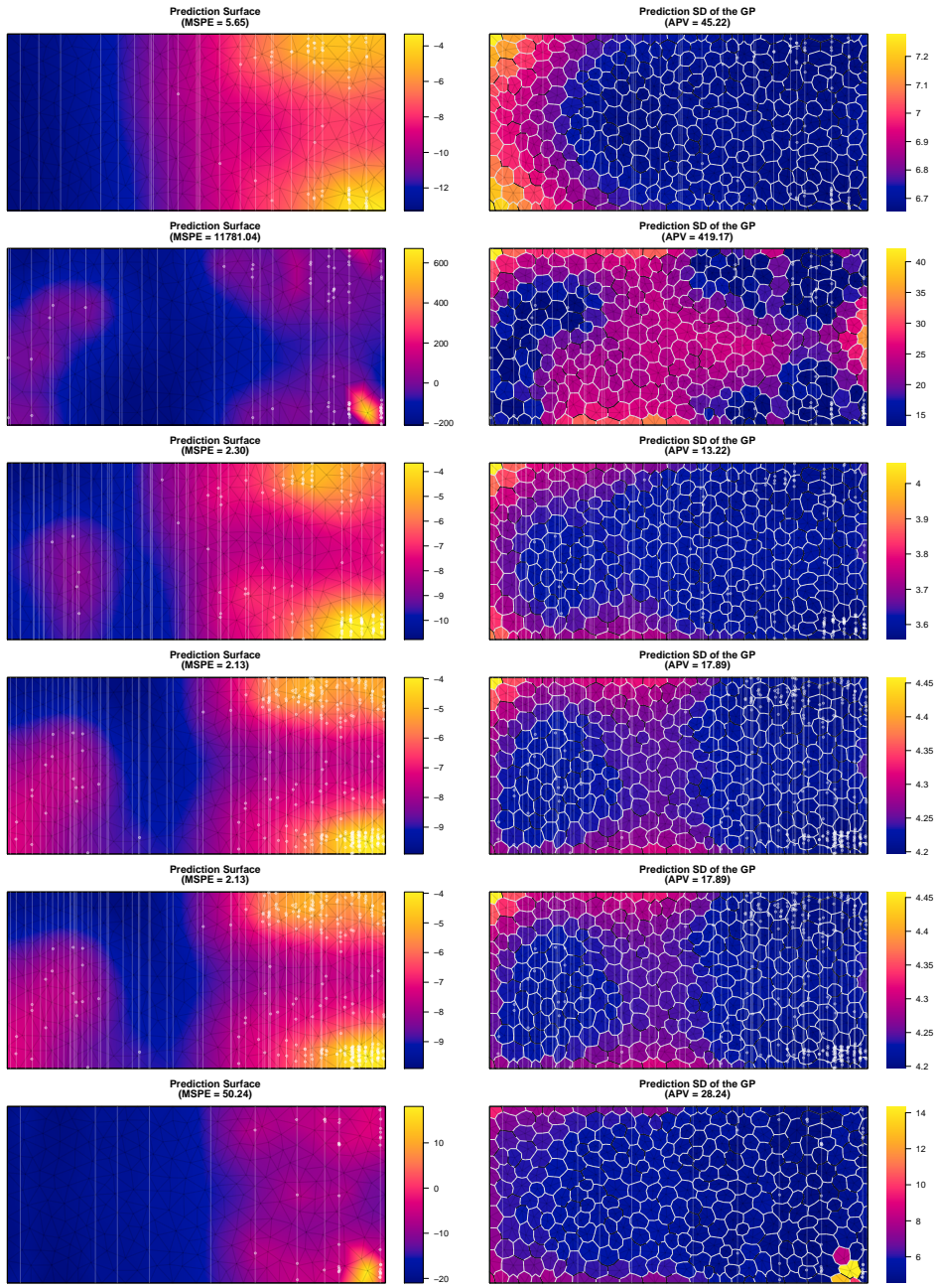


Appendix C.3. Max-MSPE surfaces, LGCP dataset

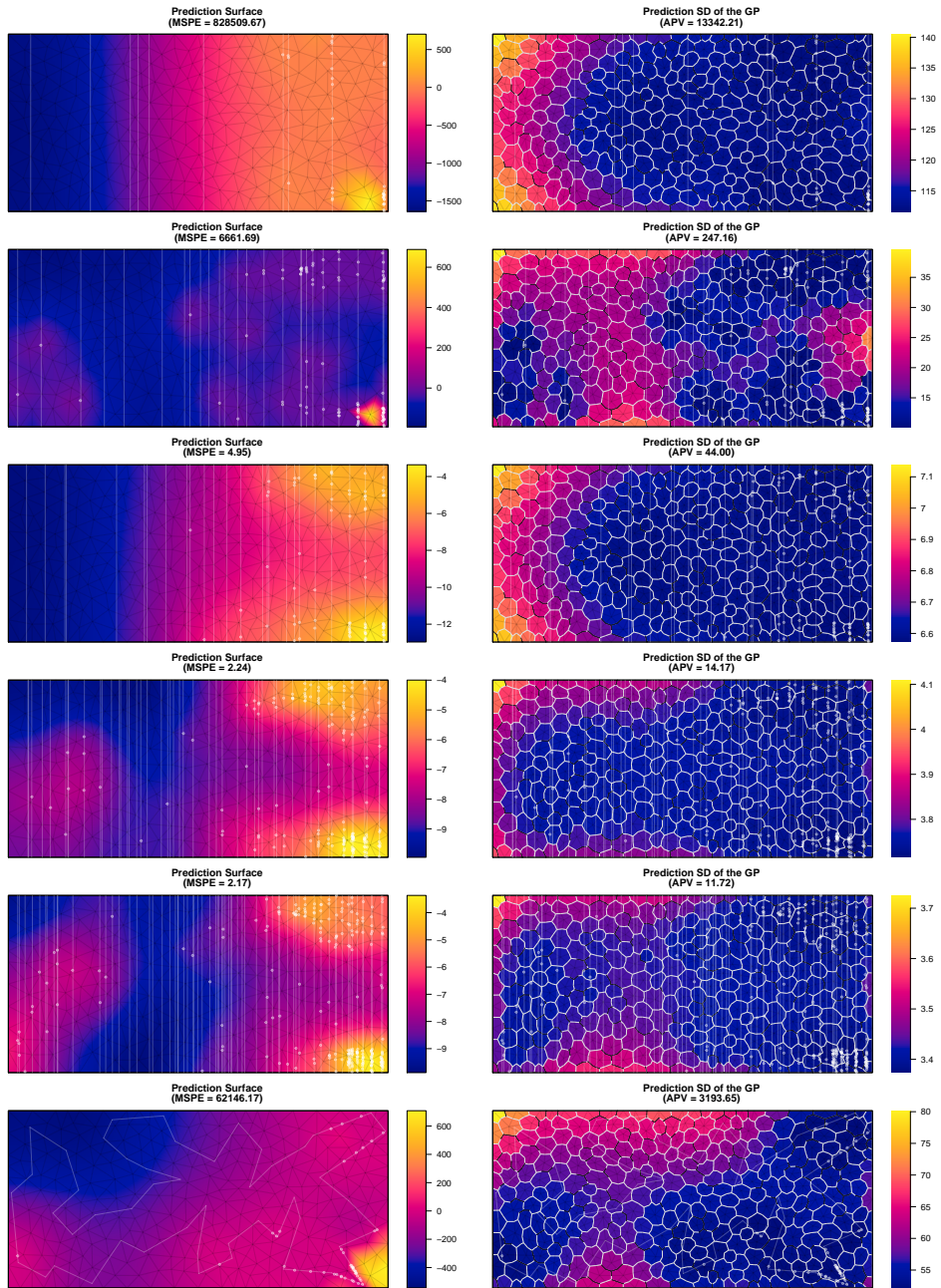




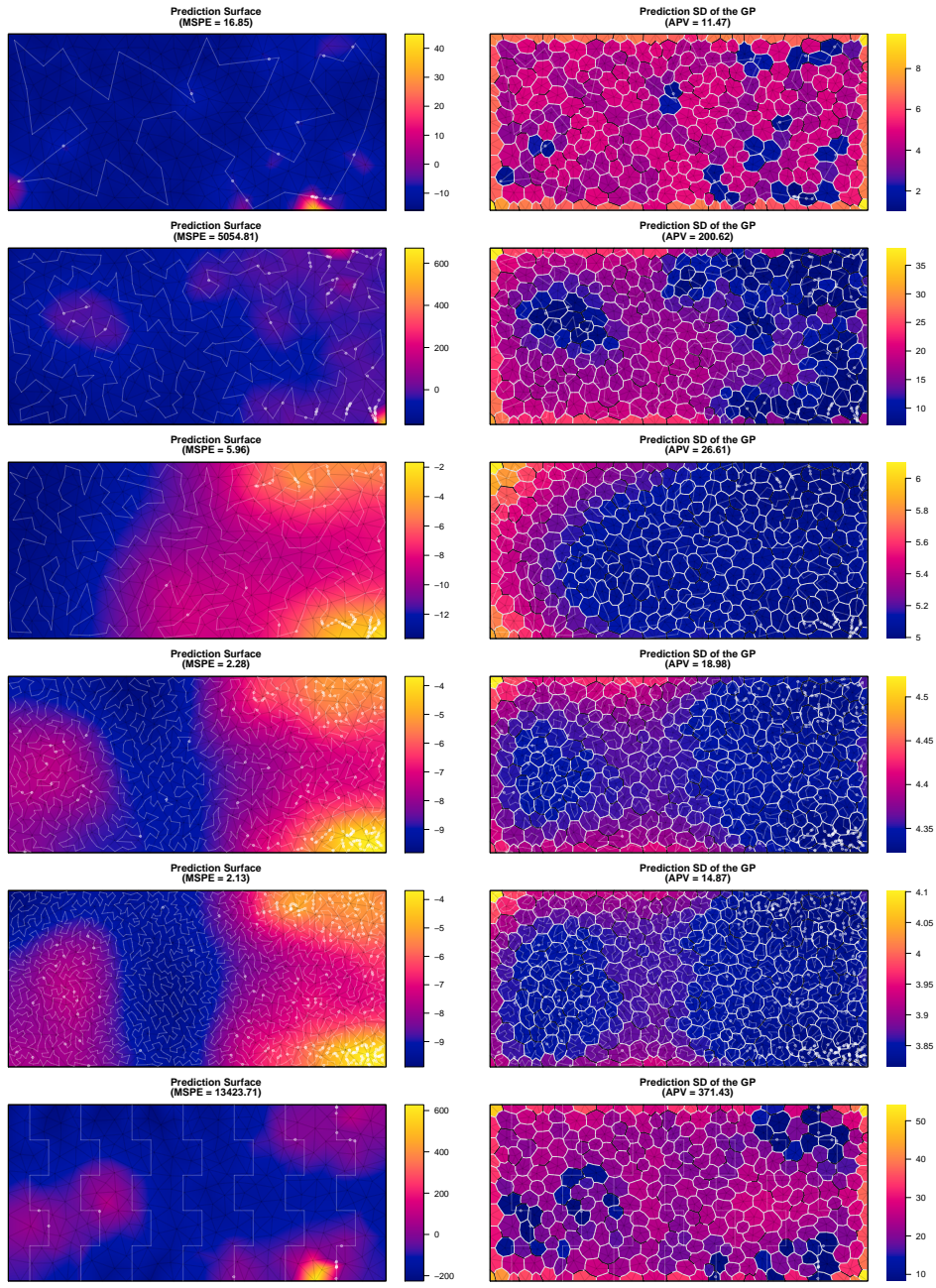
570



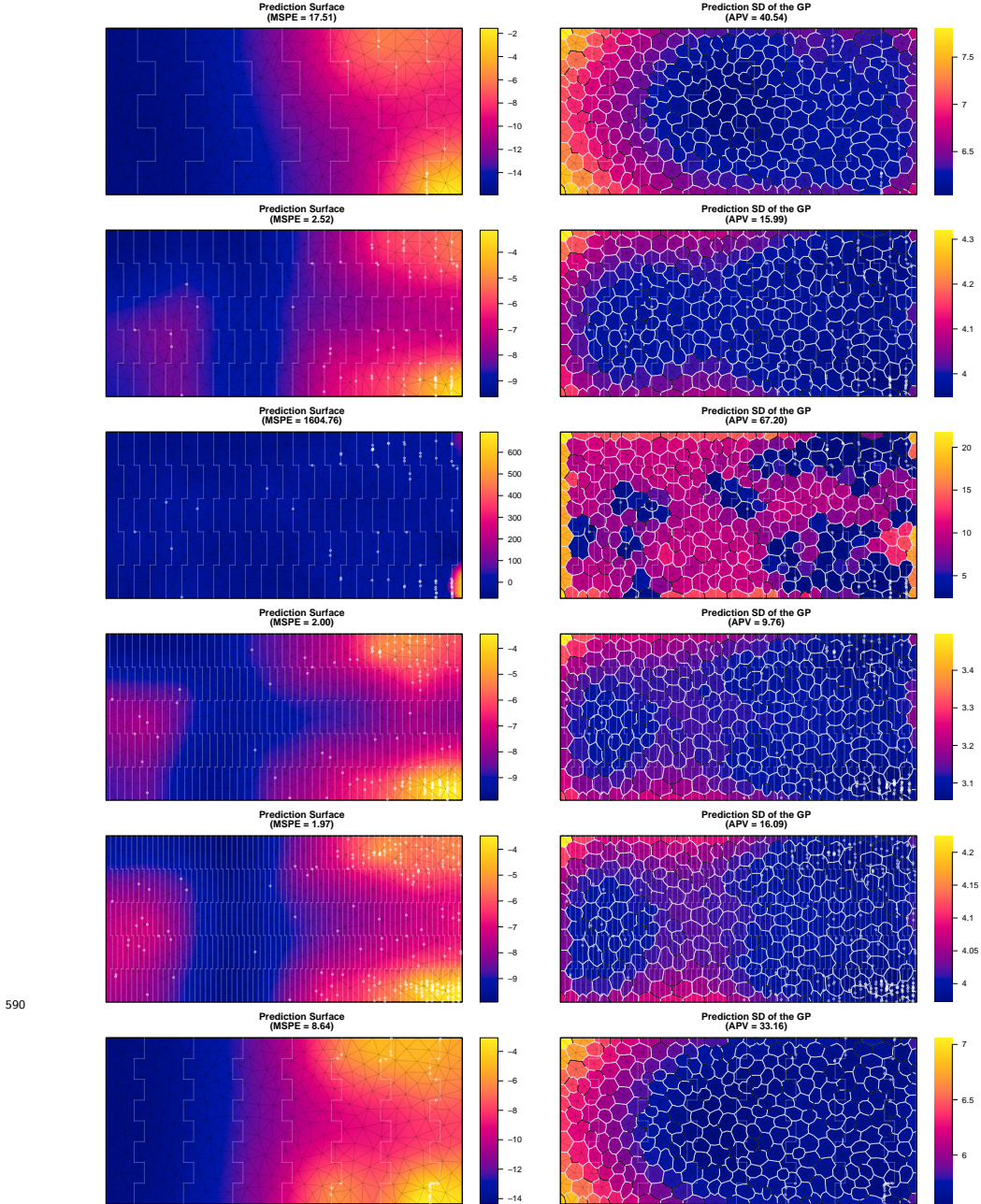
575



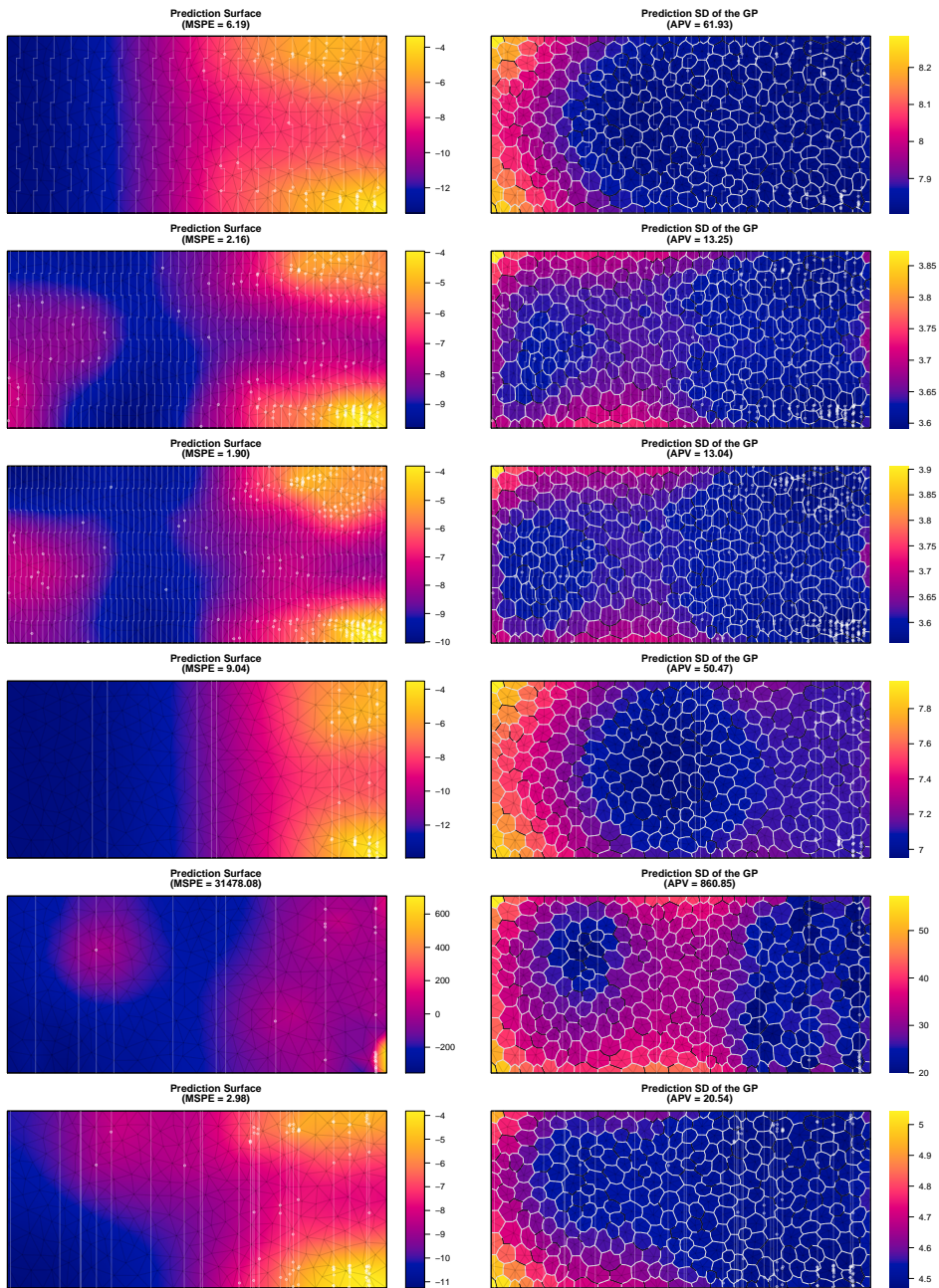
580

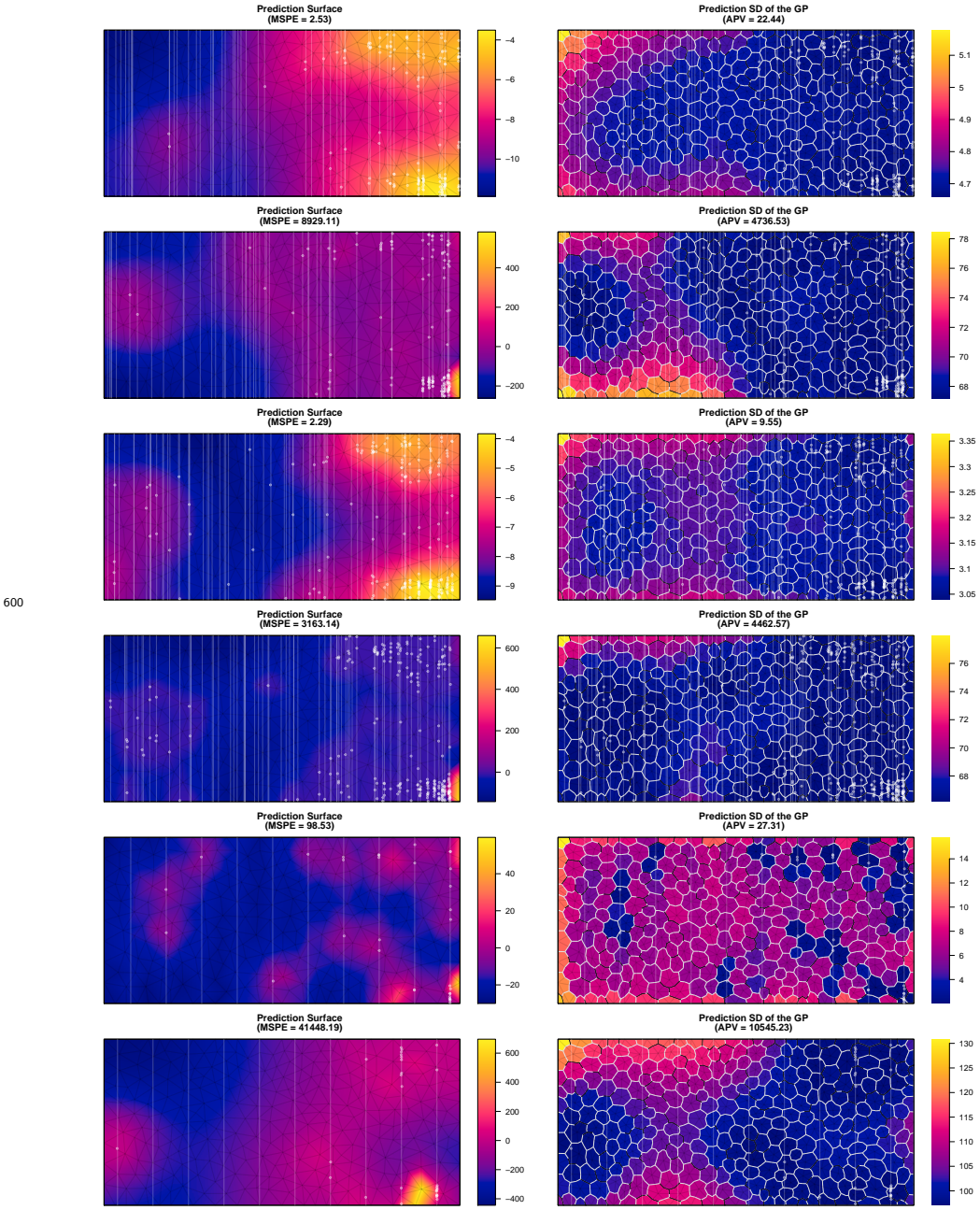


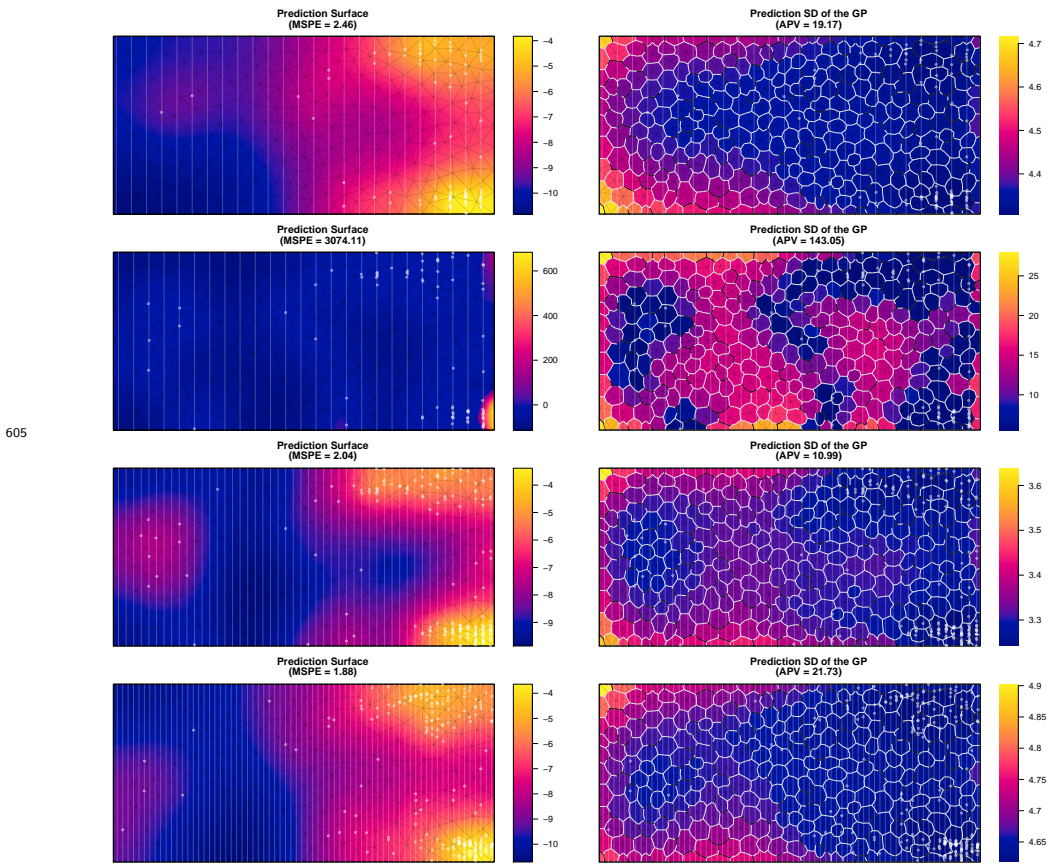
585



595







References

- Anders, S., 2009. Visualisation of genomic data with the Hilbert curve. *Bioinformatics* doi:10.1093/bioinformatics/btp152.
- Blangiardo, M., Cameletti, M., 2015. Spatial and Spatio-temporal Bayesian Models with R-INLA. Wiley.
- Borkowski, J.J., Piepel, G.F., 2009. Uniform designs for highly constrained mixture experiments. *Journal of Quality Technology* 41, 35–47.
- Carnell, R., 2020. lhs: Latin Hypercube Samples. URL: <https://CRAN.R-project.org/package=lhs>. R package version 1.0.2.
- Chakraborty, A., Gelfand, A.E., Wilson, A.M., Latimer, A.M., Silander, J.A., 2011. Point pattern modelling for degraded presence-only data over large regions. *Journal of the Royal Statistical Society: Series C (Applied Statistics)* 60, 757–776.
- Chipeta, M., Terlouw, D., Phiri, K., Diggle, P., 2017. Inhibitory geostatistical designs for spatial prediction taking account of uncertain covariance structure. *Environmetrics* 28.
- Diggle, P., Lophaven, S., 2006. Bayesian geostatistical design. *Scandinavian Journal of Statistics* 33, 53–64.
- Fan, J.A., Yeo, W.H., Su, Y., Hattori, Y., Lee, W., Jung, S.Y., Zhang, Y., Liu, Z., Cheng, H., Falgout, L., Bajema, M., Coleman, T., Gregoire, D., Larsen, R.J., Huang, Y., Rogers, J.A., 2014. Fractal design concepts for stretchable electronics. *Nature communications* 5, 3266.
- Flagg, K.A., Hoegh, A., Borkowski, J.J., 2020. Modeling partially surveyed point process data: Inferring spatial point intensity of geomagnetic anomalies. *Journal of Agricultural, Biological and Environmental Statistics* 25, 186–205.

- Fuglstad, G.A., Simpson, D., Lindgren, F., Rue, H., 2019. Constructing priors that penalize the complexity of Gaussian random fields. *Journal of the American Statistical Association* 114, 445–452.
- Hahsler, M., Hornik, K., 2020. TSP: Traveling Salesperson Problem (TSP). URL: <https://CRAN.R-project.org/package=TSP>. R package version 1.1-10.
- Husslage, B.G., Rennen, G., Van Dam, E.R., Den Hertog, D., 2011. Space-filling latin hypercube designs for computer experiments. *Optimization and Engineering* 12, 611–630.
- Illian, J.B., Sørbye, S.H., Rue, H., 2012. A toolbox for fitting complex spatial point process models using integrated nested laplace approximation (inla). *The Annals of Applied Statistics* , 1499–1530.
- Johnson, D., Laake, J., VerHoef, J., 2014. DSpat: Spatial Modelling for Distance Sampling Data. URL: <https://CRAN.R-project.org/package=DSpat>. R package version 0.1.6.
- Johnson, M.E., Moore, L.M., Ylvisaker, D., 1990. Minimax and maximin distance designs. *Journal of statistical planning and inference* 26, 131–148.
- Kelly, F.P., Ripley, B.D., 1976. A note on Strauss's model for clustering. *Biometrika* 63, 357–360.
- Lark, R., 2016. Multi-objective optimization of spatial sampling. *Spatial Statistics* 18, 412–430.
- Lindgren, F., Rue, H., Lindström, J., 2011. An explicit link between Gaussian fields and Gaussian Markov random fields: the stochastic partial differential equation approach. *Journal of the Royal Statistical Society: Series B (Statistical Methodology)* 73, 423–498.
- Liu, J., Vanhatalo, J., 2020. Bayesian model based spatiotemporal survey designs and partially observed log Gaussian Cox process. *Spatial statistics* 35, 100392.

- Ma, Q., Zhang, Y., 2016. Mechanics of fractal-inspired horseshoe microstructures for applications in stretchable electronics. *Journal of Applied Mechanics* 83.
- Matzke, B., Wilson, J., Newburn, L., Dowson, S., Hathaway, J., Sego, L.,
665 Bramer, L., Pulsipher, B., 2014. Visual Sample Plan Version 7.0 User's Guide. Pacific Northwest National Laboratory. Richland, Washington. URL: <http://vsp.pnnl.gov/docs/PNNL-23211.pdf>.
- McKay, M.D., Beckman, R.J., Conover, W.J., 1979. Comparison of three methods for selecting values of input variables in the analysis of output from a computer code. *Technometrics* 21, 239–245.
670
- Møller, J., Syversveen, A.R., Waagepetersen, R.P., 1998. Log Gaussian Cox processes. *Scandinavian journal of statistics* 25, 451–482.
- Ogorzałek, M.J., 2009. Fundamentals of fractal sets, space-filling curves and their applications in electronics and communications, in: Intelligent Computing Based on Chaos. Springer, pp. 53–72.
675
- Pollard, J., Palka, D., Buckland, S., 2002. Adaptive line transect sampling. *Biometrics* 58, 862–870.
- R Core Team, 2020. R: A Language and Environment for Statistical Computing. R Foundation for Statistical Computing. Vienna, Austria. URL: <https://www.R-project.org/>.
680
- Rue, H., Martino, S., Chopin, N., 2009. Approximate Bayesian inference for latent Gaussian models by using integrated nested Laplace approximations. *Journal of the royal statistical society: Series b (statistical methodology)* 71, 319–392.
- Sagan, H., 1994. Space-filling curves. Springer.
685
- Simpson, D., Illian, J.B., Lindgren, F., Sørbye, S.H., Rue, H., 2016. Going off grid: Computationally efficient inference for log-Gaussian Cox processes. *Biometrika* 103, 49–70.

- Simpson, D., Rue, H., Riebler, A., Martins, T.G., Sørbye, S.H., et al., 2017.
- 690 Penalising model component complexity: A principled, practical approach to
constructing priors. *Statistical science* 32, 1–28.
- Strauss, D.J., 1975. A model for clustering. *Biometrika* 62, 467–475.
- USACE, 2015. Technical Guidance for Military Munitions Response Actions. Technical Report EM 200-1-15. United States Army Corps of Engineers. URL: http://www.publications.usace.army.mil/Portals/76/Publications/EngineerManuals/EM_200-1-15.pdf.
- 695 Yuan, Y., Bachl, F.E., Lindgren, F., Borchers, D.L., Illian, J.B., Buckland, S.T.,
Rue, H., Gerrodette, T., et al., 2017. Point process models for spatio-temporal
distance sampling data from a large-scale survey of blue whales. *The Annals
700 of Applied Statistics* 11, 2270–2297.